Tube diameter in tightly entangled solutions of semiflexible polymers

David C. Morse
Department of Chemical Engineering and Materials Science, University of Minnesota, 421 Washington Ave. SE, Minneapolis, Minnesota 55455

(Received 27 December 1999; revised manuscript received 10 July 2000; published 27 February 2001)

A statistical mechanical treatment is given of the confinement of a wormlike polymer in an entangled solution to a tube, yielding quantitative predictions for the average tube diameter D_e and macroscopic plateau modulus G, in the tightly entangled regime in which D_e is much less than the persistence length L_p. Three approaches are pursued. A self-consistent binary collision approximation, which explicitly describes the topological constraints imposed by neighboring chains, yields predictions consistent with the scaling laws $D_e \propto \rho^{-3/5}$ and $G \propto \rho^{7/5}$ proposed previously, where ρ is the contour length per unit volume. An effective medium approximation, which treats the network as a continuum with a modulus G, instead yields $D_e \propto \rho^{-1/3}$ and $G \propto \rho^{4/3}$, which is found to be the correct scaling in the limit $\rho L_p^2 \gg 1$. An elastic network approximation treats the displacement of a test chain as the sum of a collective displacement of the network, which is treated as a continuum, plus a local displacement, which is treated in a binary collision approximation. Predictions are compared to measurements of both D_e and G in actin protein filament (F-actin) solutions.

DOI: 10.1103/PhysRevE.63.031502 PACS number(s): 83.10.Kn, 47.50.+d, 87.15.Aa, 87.16.Ka

I. INTRODUCTION

Several theoretical studies have discussed the dynamics [1–4] and viscoelasticity [5–14] of very highly entangled solutions of semiflexible polymers. Interest in this subject has been motivated in part by experimental studies of solutions of actin protein filaments (F-actin). F-actin has simultaneously been of interest to biologists as a major constituent of the cellular cytoskeleton, and to physicists as a model system of semiflexible polymers. Sufficiently concentrated solutions of F-actin and other similarly long, stiff polymers can form an entangled state in which each polymer is effectively confined to a tube (over periods of time less than a reptation time) in which the tube diameter D_e and entanglement length L_e are both much less than either the persistence length L_p or contour length L of the polymers. I have referred to such solutions [10–13] as ''tightly entangled'' solutions of wormlike chains, to distinguish them from the more familiar case of ''loosely entangled'' solutions typical for solutions and melts of flexible polymers, in which the tube diameter and entanglement contour length are both significantly larger than the persistence length.

The tube model developed in [11,12] to describe the tightly entangled regime requires as an input parameter a value for the tube diameter or the entanglement length, as does the original Doi-Edwards tube model of flexible or loosely entangled chains [15]. In both regimes, the value provided for D_e or L_e directly determines the value predicted for the plateau modulus by the appropriate tube model. There is thus far no quantitative molecular theory for the absolute magnitude of the tube diameter or plateau modulus in loosely entangled solutions or melts of flexible chains, although scaling laws have been developed to describe the dependence of the plateau modulus upon polymer concentration in solutions of both good [16,17] and θ solvents [18,19], and upon geometrical properties of the chain in the melt [20].

In this paper, I attempt to give a quantitative theoretical treatment of the forces confining each polymer to a tube in tightly entangled solutions, and thereby predict values for the tube diameter and plateau modulus in such solutions. The paper is organized as follows. Section II presents operational definitions of the tube diameter, the entanglement length, and the effective confinement potential for a single tightly entangled polymer, and relates these microscopic quantities to the predictions of Refs. [11,12,14] for the macroscopic plateau modulus. Section III contains an overview of the basic ideas and qualitative results of three different approximate calculations of the tube diameter. Details of these calculations are presented in Secs. IV–VI. Section VII contains a comparison of theoretical predictions to experimental results for F-actin solutions. Section VIII is a summary of conclusions.

II. DEFINITIONS

Consider a network of very long semiflexible chains, each of persistence length L_p and contour length L, with a density ρ of polymer contour length per unit volume. The conformation of a single chain may be described by a contour $\mathbf{r}(s)$, where s is a contour distance measured from one end of the chain. The bending energy is given by the wormlike chain model,

$$U_{bend}[\mathbf{r}] = \tfrac{1}{2} T L_p \int_0^L ds \left| \frac{\partial^2 \mathbf{r}(s)}{\partial s^2} \right|^2 . \tag{1}$$

Here and in what follows, temperature T is measured in units of energy, so that $k_B \equiv 1$. The chains are constrained to be inextensible by requiring that $|\partial \mathbf{r}(s)/\partial s| = 1$, and are treated throughout this paper as uncrossable but infinitely thin threads.

I focus here on a tightly entangled concentration regime in which the geometrical mesh size $L_m \equiv \rho^{-1/2}$ is much less than L_p, and in which the tube diameter and entanglement length are also expected [11] to be much less than L_p. It is assumed that each chain in a tightly entangled solution is

effectively confined to a tubelike region over time scales much less than a reptation time τ_{rep}. In the limit of very long chains, and correspondingly long reptation times, the topological structure of a network of uncrossable chains may be treated as if it were permanent for the purpose of describing averages of chain conformations over shorter times. Two different kinds of statistical average are used in what follows to describe this situation. A thermal equilibrium average for a network of some specified topology, denoted by $\langle \cdots \rangle$, is given by a Boltzmann-weighted average over all topologically accessible microscopic configurations of the network. By ''topologically accessible'' configurations, I mean those that can be deformed into one another without requiring chains to cut through each other, and also without requiring the system to pass over any other large energy barriers, such as that associated with forcing a chain to double over into a hairpin. This topologically constrained ensemble average will be assumed to be equivalent to a time average over times much less than the reptation time τ_{rep} but much greater than an entanglement time, which is (roughly) the time required for local equilibration of transverse fluctuations of the polymer within its tube. In addition, one may define an average over all possible network topologies, denoted by $\overline{\cdots}$. When calculating averages over periods of time less than the reptation time, the average over network topologies may be treated as an average over a quenched random variable.

In what follows, I consider a hypothetical situation in which a physically entangled solution is first allowed to come to an initial state of topologically unconstrained thermal equilibrium, by relaxing over many reptation times, before any averages are evaluated or external forces (discussed below) are applied to the system. Thermal averages evaluated in the initial unperturbed equilibrium state will be denoted by $\langle \cdots \rangle_0$. The double average $\overline{\langle \cdots \rangle_0}$ in this initial state must be rigorously equivalent, for chains with negligible excluded volume, to the thermal equilibrium average of an ideal solution of completely noninteracting ''phantom'' chains: When the interactions between chains have an infinitesimal range, they exclude only an infinitesimal fraction of the configuration space of the solution, and so can have no effect upon any equilibrium average, even though they drastically alter the solution's dynamics.

To characterize the constrained fluctuations of a single polymer, I focus attention upon a single randomly chosen ''test'' chain within a network of $N+1$ chains, which is surrounded by N other ''medium'' chains. The contour of the test chain is given by a vector $\mathbf{r}(s)$, where s is a distance measured along its contour. I consider how the distribution of contours for such a test chain would be affected by a hypothetical external transverse force $\mathbf{f}(s)$ that acts only on the test chain. I imagine that this force is applied only after the system has reached its initial equilibrium state, and is then held fixed over a period much less than a reptation time, during which the topology remains fixed. The probability of finding any specified network topology is thus the same in the presence of this external force as that in the initial equilibrium state. This probability is, in turn, equal to the probability that a network of the specified topology would be generated by a hypothetical process in which one took an equilibrated solution of phantom chains and suddenly turned on the constraint of uncrossability.

The thermal average $\langle \mathbf{r}(s) \rangle$ of the test chain contour (i.e., the average over times much less than the reptation time) will be referred to in what follows as the tube contour of the test chain, and the average contour $\langle \mathbf{r}(s) \rangle_0$ obtained in the absence of any external force as the unperturbed tube contour. Transverse displacements of the actual test chain contour $\mathbf{r}(s)$ from the unperturbed tube contour are characterized by a two-dimensional (2D) tranverse displacement vector

$$\mathbf{h}(s) \equiv \mathbf{r}(s) - \langle \mathbf{r}(s) \rangle_0, \tag{2}$$

which is constructed perpendicular to $\langle \mathbf{r}(s) \rangle_0$, so that $\mathbf{h}(s) \cdot \partial \langle \mathbf{r}(s) \rangle_0 / \partial s = 0$. The potential energy associated with the external force $\mathbf{f}(s)$ may be written as an integral,

$$U_{ext} \equiv -T \int ds\, \mathbf{h}(s) \cdot \mathbf{f}(s). \tag{3}$$

The total potential energy of the network in the presence of this external potential is given by the sum of the bending energies of the test chain and of all the medium chains, plus U_{ext}.

A. Transverse fluctuations

To characterize transverse fluctuations of a polymer within its tube, one may focus attention on a section of tube of some length much less than L_p but much greater than L_e, within which the tube tangent $\partial \langle \mathbf{r}(s) \rangle / \partial s$ remains nearly constant. Within such a segment, $\mathbf{h}(s)$ may be decomposed into two Cartesian components $\mathbf{h}(s) = (h_1(s), h_2(s))$ associated with the two directions perpendicular to the local tube tangent, with corresponding Fourier amplitudes

$$h_\alpha(q) \equiv \int ds e^{iqs} h_\alpha(s) \tag{4}$$

for Cartesian indices $\alpha = 1,2$. The variance of $\mathbf{h}(q)$ in the absence of any external force, averaged over both thermal fluctuations and network topologies, may be expressed as a function of the form

$$\overline{\langle h_\alpha(q) h_\beta(-q) \rangle_0} = \frac{T}{TL_p q^4 + \gamma(q)} \delta_{\alpha\beta}. \tag{5}$$

The denominator of the right hand side (rhs) may be interpreted as a spring constant for transverse modes of wave number q, in which $TL_p q^4$ is a contribution arising from the bending energy of the test chain, and $\gamma(q)$ is an as-yet-undetermined, q-dependent effective spring constant that is introduced to characterize the confinement forces arising from collisions with other polymers.

The width of the tube may be characterized by the variance

$$R_e^2 \equiv \overline{\langle h_\alpha^2(s) \rangle_0} \tag{6}$$

of either of the two Cartesian components of $\mathbf{h}(s)$ at a randomly chosen point on a randomly chosen chain, which is given by the Fourier integral

$$R_e^2 = \int \frac{dq}{2\pi} \frac{T}{TL_p q^4 + \gamma(q)}. \tag{7}$$

In what follows, I refer to the standard deviation R_e as the tube radius. The tube diameter D_e defined in Refs. [11,12] is just $2R_e$.

The entanglement contour length L_e may be defined roughly by requiring that the fluctuations of transverse modes of wave number $q \gg L_e^{-1}$ are controlled primarily by the bending energy in Eq. (7), so that $L_p q^4 \gg \gamma(q)$ for $qL_e \gg 1$, while fluctuations of modes with $q \ll L_e^{-1}$ are controlled primarily by confinement forces, so that $L_p q^4 \ll \gamma(q)$ for these longer wavelength modes. This length, which was referred to as a ''deflection length'' by Odijk [1], may also be interpreted heuristically as a distance between collisions of the polymer with the ''walls'' of a confining tube. The tube radius and entanglement (or deflection) length vary with an approximate power law relationship [1],

$$L_e \sim R_e^{2/3} L_p^{1/3}. \tag{8}$$

In the concentration regime of interest here, where $R_e \ll L_p$, this yields a hierarchy $R_e \ll L_e \ll L_p$.

B. Plateau modulus

We will be interested in what follows in predicting values for the macroscopic plateau modulus of the network as well as the tube radius and related microscopic quantities. To calculate a modulus, one must complete two largely independent steps. The first, which was attempted in Refs. [11,12,14], is to calculate the macroscopic plateau modulus from a tube model in which the fluctuations of the polymer within the tube are characterized by an unspecified function $\gamma(q)$, as above. The second, which is attempted here, is to calculate $\gamma(q)$ by considering the statistical mechanics of a network of uncrossable chains.

The calculation of the modulus given in Refs. [11,12] was based on the following physical assumptions. (i) The plateau modulus of a tightly entangled solution, in the absence of cross-links between chains, arises from the intramolecular curvature stress defined in Ref. [11]. (ii) The tube contour (i.e., thermal average contour) of each chain deforms affinely under infinitesimal macroscopic deformations of the network. (iii) The magnitude of the transverse fluctuations of the polymer about its tube contour is unchanged by such deformations, i.e., the same function $\gamma(q)$ is used to characterize transverse fluctuations in the equilibrium and infinitesimally deformed states.

The main elements in this calculation are (i) the derivation of an expression for the stress arising from a single chain with a known distribution of chain contours, which is given in Appendix A of Ref. [11], (ii) the calculation of the thermal average of this stress for a chain that is confined to undergo small transverse fluctuations about a specified tube contour, which is given in Appendix B of the same paper, and (iii) the calculation of the average stress induced by an infinitesimal affine deformation of an initially equilibrium distribution of tube contours, which is given in Appendixes B and C of Ref. [12]. The plateau modulus obtained in this series of calculations was shown to arise physically from deformation of the equilibrium distribution of tube contour curvatures, and so is referred to here as G_{curve}. Subject to the above assumptions, the calculation was carried out exactly, and yields

$$G_{curve} = \frac{7}{5} \frac{\rho T}{L_e}, \tag{9}$$

where the inverse entanglement length $1/L_e$ is defined for this purpose by a Fourier integral

$$\frac{1}{L_e} \equiv \int \frac{dq}{2\pi} \frac{\gamma(q)}{TL_p q^4 + \gamma(q)}. \tag{10}$$

This definition of L_e will be retained throughout this paper.

In Ref. [14], the calculation of the plateau modulus was extended by relaxing assumption (iii), and thus allowing for the possibility that the cross-sectional dimensions of the tube, as characterized by the elements of the tensor $\overline{\langle h_\alpha(q) h_\beta(-q) \rangle}$, may also change in response to a macroscopic deformation. It was shown there that if assumption (iii) is abandoned, then the plateau modulus may in general be expressed as a sum

$$G = G_{curve} + G_{dilate} \tag{11}$$

of the ''tube curvature'' contribution G_{curve} given above, which arises from affine deformation of the thermal average chain contour, plus an additional ''tube dilation'' contribution, which arises instead from disturbance of the equilibrium distribution of transverse fluctuations of the polymer contour about its average. Both contributions originate in the intramolecular curvature stress of the polymer [assumption (i)], but arise from different kinds of tube deformation. To estimate the maximum plausible magnitude of the tube dilation contribution, G was recalculated in Ref. [14] under the assumption that the cross-sectional dimensions of the tube (defined in terms of the variance of h) as well as the tube contour undergo strictly affine deformation. This was found to yield a tube dilation contribution

$$G_{dilate} \simeq \frac{1}{5} \frac{\rho T}{L_e}, \tag{12}$$

which must be added to the value of G_{curve} given in Eq. (9).

Upon comparing Eqs. (12) and (9), we see that, while both contributions to G are of order T per entanglement, the numerical prefactor obtained for G_{dilate} happens to be seven times smaller than that obtained for G_{curve}. If the deformation of the tube contour is at all close to affine, we thus expect the modulus to be numerically dominated by the tube curvature contribution, whether or not there is also a signficant degree of anisotropic tube dilation. Conversely, if the

deformation of the tube contour is far from affine, refinement of our treatment of the contribution of anisotropic tube dilation is unlikely to save the theory from quantitative failure. For simplicity, when comparing theoretical predictions for G to measurements on F-actin, I use Eq. (9) alone for the plateau modulus, thus ignoring any possible anisotropic tube dilation, while keeping in mind that the predicted modulus could be raised by up to about 15% by assuming the existence of such an effect. I remain agnostic on the question of whether a signficant deformation of the tube cross section will actually occur in the linear viscoelastic regime. This last question might in principle be answerable by extending the present theory so as to describe the tranverse fluctuations of a confined polymer in a macroscopically deformed network (here, I attempt only to describe fluctuations in the undeformed state), but this has not been attempted.

C. Confinement potentials

The forces that act to confine a polymer to a tube in equilibrium may be characterized by introducing two closely related single-chain thermodynamic potentials, which are defined briefly below and more formally in Appendix A.

To characterize the forces acting upon a test chain with a specified conformation in a network of specified topology, one may define a potential of mean force $A_{conf}[\mathbf{h}]$ that is a functional of the displacement field $\mathbf{h}(s)$. This quantity is given by the total free energy of the network, excluding the bending energy of the test chain, in a hypothetical situation in which the test chain is constrained to follow a specified contour $\mathbf{r}(s)$. The potential of mean force is thus defined by treating the test chain as an uncrossable, unmoveable threadlike obstacle, and integrating over all topologically accessible states of the surrounding network of medium chains. The thermal average of the transverse confinement force $f_{conf}(s)$ exerted by the test chain upon surrounding chains via collisions at point s is given by the functional derivative

$$\langle f_{conf,\alpha}(s)\rangle = \frac{\delta A_{conf}[\mathbf{h}]}{\delta h_\alpha(s)}, \tag{13}$$

where $\langle\cdots\rangle$ refers here to a thermal average over fluctuations of the surrounding network of medium chains, and where $f_{conf,\alpha}(s)$ and $h_\alpha(s)$ are Cartesian components of the transverse fields $\mathbf{f}_{conf}(s)$ and $\mathbf{h}(s)$, respectively.

To instead characterize the forces experienced by a fluctuating semiflexible chain within a network of unspecified topology, I consider a situation in which the test chain is allowed to fluctuate, but is subjected to a known transverse force $\mathbf{f}(s)$ that yields a corresponding average transverse displacement $\overline{\langle\mathbf{h}(s)\rangle}$. It is shown in Appendix A that the quantity $\gamma(q)$, which is implicitly defined by Eq. (5) for $\overline{\langle h_\alpha(q)h_\beta(-q)\rangle_0}$, may also be expressed as a functional derivative

$$\gamma(q) = \left.\frac{\overline{\langle f_{conf,\alpha}(q)\rangle}}{\delta\overline{\langle h_\alpha(q)\rangle}}\right|_{\overline{\langle\mathbf{h}\rangle}=0}, \tag{14}$$

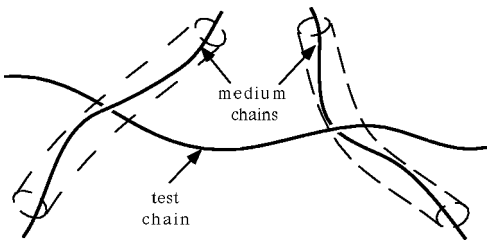

FIG. 1. Schematic of a semiflexible test chain embedded in a network of uncrossable medium chains, each of which is itself confined to a tube as a result of constraints imposed by other medium chains.

where $f_{conf,\alpha}(q)$ and $h_\alpha(q)$ are Fourier components of $f_{conf,\alpha}(s)$ and $h_\alpha(s)$, respectively. In Appendix A, I introduce an effective confinement potential $\Gamma_{conf}[\overline{\langle\mathbf{h}\rangle}]$ for this situation, which is the functional Legendre transform of $\overline{A_{conf}[\mathbf{h}]}$, and which may be defined by the requirement that

$$\overline{\langle f_{conf,\alpha}(q)\rangle} = \frac{\delta\Gamma_{conf}}{\delta\overline{\langle h_\alpha(q)\rangle}}. \tag{15}$$

By differentiating both sides of Eq. (15) with respect to $\overline{\langle h_\alpha(-q)\rangle}$ and comparing to Eq. (14), we see that

$$\gamma(q) = \left.\frac{\delta^2\Gamma_{conf}}{\delta\overline{\langle h_\alpha(q)\rangle}\,\delta\overline{\langle h_\alpha(-q)\rangle}}\right|_{\overline{\langle\mathbf{h}\rangle}=0}. \tag{16}$$

A self-consistent approximation for $\gamma(q)$ may thus be formulated as an approximation for the effective confinement potential $\Gamma_{conf}[\overline{\langle\mathbf{h}\rangle}]$.

III. OVERVIEW

To calculate Γ_{conf}, we must consider the situation shown schematically in Fig. 1, in which a randomly chosen test chain is embedded in a network, and estimate the transverse force $\mathbf{f}(s)$ required to displace the test chain by a specified average displacement $\overline{\langle\mathbf{h}(s)\rangle}$. The forces opposing displacement of the test chain are the result of collisions with a relatively small number of nearby medium chains whose tube contours happen to pass within a distance of order R_e of the test chain. Any estimate of the average displacement of the test chain in response to a specified force must rely upon a corresponding estimate of the ease with which these nearby medium chains may be displaced by forces exerted upon them by the test chain. To construct a self-consistent statistical mechanical theory, one must require that the degree of mechanical compliance assumed for the medium chains be consistent with the mechanical compliance $1/\gamma(q)$ calculated for the test chain. In Secs. IV–VI, I present three different self-consistent calculations of $\gamma(q)$, based upon different simplifying approximations for the mechanical compliance of the network of surrounding medium chains. Before plunging into details, an overview of the physical content and qualitative results of each approximation is given below.

A. Binary collision approximation

The binary collision approximation (BCA) of Sec. IV gives a rather detailed description of the interaction of the test chain with individual nearby medium chains, but neglects any effects arising from the collective elastic relaxation of the network. In the BCA, we imagine that the test chain is embedded in a thicket of uncrossable but slightly mobile medium chains. It is assumed that, in the absence of the test chain, each of the medium chains would itself remain confined to a tube as a result of its interactions with other medium chains, and that the net effect of these interactions between medium chains may be mimicked by a harmonic potential that (in the absence of the test chain) would confine each medium chain to fluctuate about a preferred tube contour. The presence of the test chain then acts to further constrain the fluctuations of the medium chain within its tube, by forcing the medium chain to remain trapped on one side or the other of the test chain. This constraint may be expressed as a constraint on the range of allowed values for the transverse displacement of the medium chain from its preferred tube contour at the point where the test chain passes closest to the tube contour of the medium chain. The free energy associated with the interaction of the test chain with a single such medium chain is given by the increase in the fluctuation free energy of the medium chain arising from this topological constraint. An effective confinement potential for the test chain is obtained by calculating an appropriate average of this binary interaction free energy over all possible orientations and positions of the tube contours of nearby medium chains. The calculation is made self-consistent by requiring that the value of $\gamma(q)$ thereby calculated for the test chain (which, in this approximation, is actually independent of q) equal that assumed for the surrounding medium chains.

The BCA is found to yield an expression for the tube radius R_e with the same power law dependences on ρ and L_p as those predicted by Semenov on the basis of a simple geometrical argument [3]. Semenov's argument amounted to the assumption that of order one medium chain should pierce the tube of the test chain per entanglement contour length. The argument may be restated, using reasoning closer to that followed in Sec. IV, as follows: To estimate γ, consider the free energy required to displace the test chain by an average distance $\langle h \rangle$ of order the tube radius R_e. Such a displacement will significantly alter the topological constraints experienced by all medium chains whose tube contour passes within a distance of order R_e of the unperturbed test chain contour. Assuming a free energy cost of order T for each such nearby chain gives a free energy of $\Gamma_{conf}/L \sim T\rho R_e$ per unit length of test chain for a displacement of this magnitude, where ρR_e is the number of chains that pierce a cylinder of radius R_e per unit length of the cylinder. If one assumes that Γ_{conf} is approximately quadratic in h, one obtains a spring constant

$$\gamma \sim T\rho/R_e . \tag{17}$$

By requiring that this expression for γ yield $\gamma \sim TL_p q^4$ for wave numbers $q \sim L_e^{-1}$, and using Eq. (8) to relate R_e and L_e, one obtains an estimated tube diameter and entanglement length

$$R_e \sim \rho^{-3/5} L_p^{-1/5},$$

$$L_e \sim \rho^{-2/5} L_p^{1/5}. \tag{18}$$

By setting $G \sim \rho T/L_e$ (i.e., T per entanglement), one obtains a corresponding modulus

$$G \sim T\rho^{7/5} L_p^{-1/5}. \tag{19}$$

These scaling relations have been taken as a starting point in several recent treatments of tightly entangled solutions by this author [11–13] and several others [5,6,31].

B. Effective medium approximation

The effective medium approximation (EMA) of Sec. V starts from a very different point of view, by treating the network surrounding the test chain as an elastic continuum with a shear modulus equal to the self-consistently determined plateau modulus of the solution, and the test chain as a thread embedded in this medium. It is a straightforward exercise in continuum mechanics (presented below) to show that the elastic force resisting a sinusoidal transverse displacement of the test chain with wave number q within a medium of modulus G may be described by an effective spring constant

$$\gamma(q) \sim -G/\ln(qL_e) \tag{20}$$

that depends linearly on G and, for $qL_e \lesssim 1$, logarithmically on q, so that $\gamma(q)$ vanishes in the limit of small q.

The length L_e appears within the logarithm in Eq. (20) because it has been introduced into the continuum mechanical calculation as a short-wavelength cutoff length, thus effectively smearing the forces applied to the chain over a region with a radius of order L_e around the test chain. It is straightforward to show that, if the force on the medium is taken to be localized along a mathematical line, then the compliance $1/\gamma(q)$ diverges logarithmically (like the electrostatic potential for a line charge), signaling the breakdown of the continuum approximation at short length scales and the need for a short-wavelength cutoff. It is argued that a cutoff length of order L_e is appropriate because of the ability of single chains to directly transmit forces over distances of order the distance L_e between collisions, before effectively distributing them over the network. In Sec. V, I go somewhat beyond this qualitative argument and regularize the calculation of $\gamma(q)$ using an approximate description for the distribution of forces exerted by the few ''primary'' medium chains, which pass close enough to the test chain to collide directly with it, upon ''secondary'' medium chains, which confine the primary chains, and then use the continuum approximation only to describe the response of the surrounding network of secondary chains. The results are similar to those obtained by *ad hoc* introduction of a cutoff length of order L_e.

Self-consistent estimates of R_e and G may be obtained in the EMA by requiring that $\gamma(q) \sim G \sim L_p q^4$ for wave num-

bers $q \sim 1/L_e$, and that $G \sim \rho T/L_e$. These conditions, together with Eq. (20) for $\gamma(q)$ and Eq. (8) for L_e, yield power laws

$$R_e \sim \rho^{-1/2},$$

$$L_e \sim \rho^{-1/3} L_p^{1/3},$$

$$G \sim T \rho^{4/3} L_p^{-1/3}. \tag{21}$$

In the more detailed calculation presented in Sec. V, I substitute a value of $\gamma(q)$ that is calculated from a continuum mechanical treatment of the medium into Eqs. (9) and (10) for G, and thereby obtain an integral equation for the modulus G. The solutions of this integral equation are shown to exactly obey the scaling laws given in Eq. (21), with numerical prefactors that depend weakly (i.e., logarithmically) upon the cutoff length used to regularize the divergence of the network strain near the test chain.

Note that the EMA scaling exponents given in Eq. (21) are different from those predicted by the BCA, which are given in Eq. (18), and so are different from those assumed to be correct in all of the recent theoretical work on the sources of elasticity in these solutions. This raises the question of which theoretical approach (if either) gives the correct asymptotic scaling in the limit $\rho L_p^2 \gg 1$ that both the BCA and EMA are intended to described. Because these two approaches describe two essentially independent mechanisms for displacement of the test chain (i.e., displacement of the test chain relative to the average displacement of a partially frozen environment in the BCA and collective elastic displacement of that environment in the EMA), the tube diameter is presumably controlled by whichever mechanism predicts a larger tube diameter. In the limit ρL_p^2 of interest, the EMA prediction for the tube radius is larger than the BCA prediction by a factor proportional to $(\rho L_p^2)^{1/10}$, suggesting that it is actually the EMA that yields the correct asymptotic scaling in the limit of extremely tightly entangled chains. It is important to note, however, that the values of the exponents obtained in these two approaches are numerically quite close (e.g., $G \propto \rho^{1.33}$ vs $G \propto \rho^{1.4}$), so that the competing physical mechanisms assumed in these two approaches could remain comparable in importance at all but truly enormous values of ρL_p^2.

C. Elastic network approximation

In Sec. VI, I consider an elastic network approximation (ENA) that attempts to integrate the binary collision and effective medium approaches. In this approximation, the average displacement of the test chain in response to an external force is expressed as a sum of two contributions: (i) a local displacement of the test chain relative to its immediate environment, as defined by the tube contours of nearby medium chains, and (ii) a collective elastic displacement of the surrounding network in response to the forces exerted upon it by the test chain. The local displacement of the test chain relative to its environment is treated using the binary collision approximation, and the elastic displacement of its environment is treated in an effective medium approximation. This allows the different mechanisms of transverse displacement upon which the simpler BCA and EMA models are based to act in parallel. The resulting model is made self-consistent by requiring that the values of G and R_e obtained by using the calculated value of $\gamma(q)$ in Eq. (7) for R_e and in Eqs. (9) and (10) for G both be consistent with those used as inputs to the calculation of $\gamma(q)$. The ENA yields a tube radius that is always somewhat larger than that predicted by either the BCA or EMA separately, with no simple power law dependence on concentration. All predictions of the ENA converge to the corresponding predictions of the EMA in the limit $\rho L_p^2 \to \infty$, but remain significantly different at the values of $\rho L_p^2 \sim 10^4$ typical of recent experiments on F-actin solutions.

IV. BINARY COLLISION APPROXIMATION

In the binary collision approximation, we focus primarily on describing the interaction of the test chain and a single nearby medium chain. The contour of the medium chain of interest is denoted by $\tilde{\mathbf{r}}(\tilde{s})$, where $\tilde{s}$ is a contour length along the medium chain.

The central assumption of the BCA is that, in the absence of the test chain, each medium chain of interest would remain confined to a tube as the result of constraints imposed upon it by other medium chains. To characterize these constraints, it is useful to consider a hypothetical situation in which the test chain and a single medium chain of interest are noninteracting, and so may pass freely through one another, but in which every other pair of polymers remains mutually uncrossable and retain the same topological relationships as in the physical situation of interest. This hypothetical state will be referred to as the ''transparent state'' of the specified medium chain. The transparent state remains well defined when an external force $\mathbf{f}(s)$ is exerted on the test chain, in which case the force on the test chain must be transmitted to the network via collisions with medium chains other than the one of immediate interest. In what follows, thermal averages evaluated in the transparent state are denoted by $\langle \cdots \rangle_t$, and averages evaluated in the unperturbed transparent state, with $\mathbf{f}(s) = \mathbf{0}$, by $\langle \cdots \rangle_{t,0}$.

The thermal average $\langle \mathbf{r}(\tilde{s}) \rangle_t$ of a medium chain in its transparent state will be referred to in what follows as its preferred tube contour. (It is ''preferred'' in the sense that this is the tube contour that would be obtained if the medium chain were allowed to cut through the test chain.) Deviations of the medium chain contour from its preferred tube contour are characterized by a transverse displacement field

$$\tilde{\mathbf{h}}(\tilde{s}) \equiv \tilde{\mathbf{r}}(s) - \langle \tilde{\mathbf{r}}(\tilde{s}) \rangle_t \tag{22}$$

constructed perpendicular to the tube tangent vector $\partial \langle \tilde{\mathbf{r}}(\tilde{s}) \rangle_t / \partial \tilde{s}$. As discussed below, the presence of an uncrossable test chain acts simply to constrain the range of topologically accessible values of $\tilde{\mathbf{h}}(\tilde{s})$ at the point of closest approach between the test chain and the preferred tube contour $\langle \tilde{\mathbf{r}}(\tilde{s}) \rangle_t$.

The binary collision approximation is based upon the following simplifying approximations for the distribution of medium chain contours in the transparent state.

(i) The distribution of values of $\tilde{\mathbf{h}}(\tilde{s})$ in the transparent state is approximated by a Gaussian functional with a variance given by Eq. (5). This is equivalent to assuming that each medium chain is confined by a harmonic potential

$$A_{conf}[\tilde{\mathbf{h}}] = \int \frac{dq}{2\pi} \gamma(q) |\tilde{\mathbf{h}}(q)|^2, \tag{23}$$

with a self-consistently determined value for $\gamma(q)$.

(ii) The preferred tube contour $\langle \tilde{\mathbf{r}}(\tilde{s}) \rangle_t$ of the medium chain is taken to remain unchanged when an external force $\mathbf{f}(s)$ is exerted on the test chain, i.e., we take $\langle \tilde{\mathbf{r}}(\tilde{s}) \rangle_t = \langle \tilde{\mathbf{r}}(\tilde{s}) \rangle_{t,0}$.

Approximation (ii) is equivalent to saying that the confinement potential experienced by each medium chain in its transparent state, which represents the forces exerted upon it by other medium chains, remains unchanged when the test chain is displaced by an external force. It is this approximation that allows one to convert the many-chain problem into a tractable two-chain problem, in which we imagine that the test chain is embedded in a thicket of noninteracting medium chains, each of which fluctuates in a static harmonic potential. The same assumption also, however, prevents the BCA from taking into account any collective elastic relaxation of the surrounding network, whereby a force exerted by the test chain on one medium chain may be transmitted through the network and cause a shift in the preferred tube contour $\langle \tilde{\mathbf{r}}(\tilde{s}) \rangle_t$ of another. The binary collision approximation thus describes the fluctuations of a test chain in a partially frozen environment, in which the tube contours of the surrounding medium chains remain frozen when the test chain is displaced.

Another simplifying feature of the BCA is that the average restoring forces are nearly local functionals of $\mathbf{h}(s)$, and so may be characterized by a q-independent value for $\gamma(q)$. In the BCA, the forces on a test chain arise from collisions with medium chains whose tube contours pass close to the test chain at randomly located points along its length. Collisions between the test chain and any single medium chain are localized within a region of size R_e along either chain, which is much smaller than the typical distance L_e between collisions. Interactions between chains may thus be treated as pointlike binary interactions occurring at uncorrelated points along the test chain. Such interactions give rise to an average restoring force at each point that depends only on transverse displacement at that point, and, correspondingly, to a q-independent value for $\gamma(q)$. We may thus calculate $\gamma(q)$ in the BCA by considering only the response to a spatially uniform force $\mathbf{f}$, to obtain $\gamma(q=0)$.

In Sec. IV A, we calculate the BCA effective potential by considering the free energy required to displace a very long rigid rod inserted at random into a solution of semiflexible medium chains. The use of a long, rigid test chain simplifies the calculation, by allowing us to ignore thermal fluctuations of the test chain. A closely analogous calculation for the physically relevant case in which both the test and the medium chains are fluctuating semiflexible chains is given in Appendix B. The results of this refined calculation are discussed in Sec. IV B.

A. Confinement of a rigid test rod

To calculate the confinement potential for a rigid test rod, one may consider a hypothetical process in which a thin, uncrossable rod of length $L \ll L_e$ is first inserted into an entangled solution, the solution is then allowed to equilibrate for many reptation times while the test rod remains stationary, and the test rod is then subjected to a uniform transverse displacement $\mathbf{h}$ of magnitude $h \equiv |\mathbf{h}|$ from its initial position. The effective potential is given by the resulting increase in the free energy of the surrounding network. In the limit $L \to \infty$, we need not distinguish between the potential of mean force $A_{conf}(h)$ obtained for a rod subjected to a specified uniform displacement h and the effective potential $\Gamma_{conf}(h)$ obtained for a rod subjected to a uniform force $\mathbf{f}$ that is chosen so as to give the same average displacement $h \equiv |\overline{\langle \mathbf{h} \rangle}|$, because the heterogeneities in the local environment of the test rod become self-averaging for a sufficiently long rod, and because the spontaneous thermal fluctuations of the rod's position vanish in this limit, allowing us to treat h and $A_{conf}(h)$ as macroscopic thermodynamic variables. No equally simple statement can be made about the relationship between $A_{conf}[h]$ and $\Gamma_{conf}[\overline{\langle \mathbf{h} \rangle}]$ for a fluctuating semiflexible test chain.

Consider the interaction of a test rod $\mathbf{r}(s)$ with a nearby medium chain with a tube contour $\langle \tilde{\mathbf{r}}(\tilde{s}) \rangle_t$. The test rod is assumed to have a constant unit tangent vector $\mathbf{u}$, and to follow the straight line

$$\mathbf{r}(s) = s\mathbf{u} + \mathbf{h}, \tag{24}$$

where $\mathbf{h}$ is a uniform transverse displacement of the rod from its initial position. The tube contour of the medium chain is assumed to have a unit tangent vector $\tilde{\mathbf{u}} \equiv d\langle \tilde{\mathbf{r}}(\tilde{s}) \rangle_t / d\tilde{s}$ at the point where $\langle \tilde{\mathbf{r}}(\tilde{s}) \rangle_t$ passes its closest approach to the initial contour $\mathbf{r}(s) = s\mathbf{u}$ of the test rod. The orientations $\tilde{\mathbf{u}}$ and $-\tilde{\mathbf{u}}$ are physically indistinguishable, and so by convention we will always define $\tilde{\mathbf{u}}$ so as to give $\tilde{\mathbf{u}} \cdot \mathbf{u} \geq 0$. The preferred tube contour of the medium chain may be approximated near this point of closest approach by a straight line

$$\langle \tilde{\mathbf{r}}(\tilde{s}) \rangle_t = s_0\mathbf{u} + c_0\tilde{\mathbf{e}}_1 + \tilde{s}\,\tilde{\mathbf{u}}. \tag{25}$$

Here, $|c_0|$ is the distance of closest approach from the initial test rod contour $\mathbf{r}(s) = s\tilde{\mathbf{u}}$,

$$\tilde{\mathbf{e}}_1 \equiv \frac{\mathbf{u} \times \tilde{\mathbf{u}}}{|\mathbf{u} \times \tilde{\mathbf{u}}|} \tag{26}$$

is a unit vector constructed perpendicular to both $\mathbf{r}(s)$ and $\langle \tilde{\mathbf{r}}(\tilde{s}) \rangle_t$ at their point of closest approach, and $s_0\mathbf{u}$ is the closest point on the initial test chain contour. The distance of

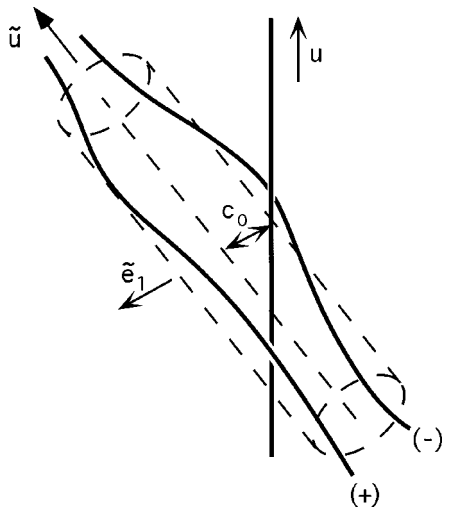

FIG. 2. Geometry for an uncrossable test rod with unit tangent vector **u** (vertical thick line) near its point of closest approach to the preferred tube contour $\langle \tilde{\mathbf{r}}(\tilde{s})\rangle_t$ with a local tangent $\tilde{\mathbf{u}}$ (dotted line along the axis of the cylindrical tube) of a nearby medium chain. Two possible contours for the fluctuating medium chain, in the + and − topological states, are shown by curved solid lines.

closest approach between $\langle \tilde{\mathbf{r}}(\tilde{s})\rangle_t$ and the displaced test rod, when $\mathbf{h}\neq\mathbf{0}$, is given by $|c|$, where

$$c \equiv c_0 - h_1 \tag{27}$$

and where $h_1 \equiv \mathbf{h}\cdot\tilde{\mathbf{e}}_1$.

In the physical situation of interest, the presence of an uncrossable test rod constrains the allowed values of $\tilde{\mathbf{h}}(\tilde{s})$ at the point of closest approach of $\mathbf{r}(s)$ and $\langle \tilde{\mathbf{r}}(\tilde{s})\rangle_t$. To describe this, it is convenient to decompose $\tilde{\mathbf{h}}(\tilde{s})$ into Cartesian components as

$$\tilde{\mathbf{h}}(\tilde{s}) = \tilde{h}_1(\tilde{s})\tilde{\mathbf{e}}_1 + \tilde{h}_2(\tilde{s})\tilde{\mathbf{e}}_2, \tag{28}$$

where $\tilde{\mathbf{e}}_2 \equiv \tilde{\mathbf{u}}\times\tilde{\mathbf{e}}_1$ is a second unit vector constructed perpendicular to $\tilde{\mathbf{u}}$. The presence of the test rod constrains the value of component $\tilde{h}_1$ at the point of closest approach to either of two possible ranges, corresponding to two different possible topological states: Either $\tilde{h}_1 > -c$, in which case the chain is trapped in what will be called the + state, or $\tilde{h}_1 < -c$, and the chain is trapped in the − state (see Fig. 2).

We may calculate the conditional probability that a medium chain with a known preferred tube contour $\langle \tilde{\mathbf{r}}(\tilde{s})\rangle_t$ will be found in the + or − topological states as follows. In the initial fully equilibrated state, with $\mathbf{h}=0$, the network is restricted to a set of microstates consistent with a certain randomly chosen topology, but the relative probabilities of different possible topologies are the same as those expected for a solution of noninteracting chains. The presence of an uncrossable test rod divides the set of microstates accessible to the system in the transparent state of a given medium chain into two subsets, corresponding to two different topologies of the network that differ only in the topological relationship of the test rod and the single medium chain of interest, which we refer to as the + and − states. The relative probabilities of finding the network in either of these two topologies are thus given by the relative probabilities of trapping the medium chain in the + or − states by a hypothetical process in which the network is first equilibrated in the transparent state and the test chain is then suddenly made uncrossable, i.e., they are given by the thermal equilibrium probabilities of finding $\tilde{h}_1 > -c$ or $\tilde{h}_1 < -c$ in the transparent state.

Let $P(\tilde{h}_1)$ denote the conditional probability that in the transparent state $\tilde{h}_1$ will take on a specified value at the point of closest approach between $\langle \tilde{\mathbf{r}}(\tilde{s})\rangle_t$ and $\mathbf{r}(s)$, for a medium chain with a known tube contour $\langle \tilde{\mathbf{r}}(\tilde{s})\rangle_t$. The corresponding conditional probability p_+ that the chain will be trapped in the + state is thus given by the probability that $\tilde{h}_1 > -c_0$ at this point in the transparent state, i.e.,

$$p_+(c_0) = \int_{-c_0}^{\infty} d\tilde{h}_1 P(\tilde{h}_1). \tag{29}$$

The corresponding probability of finding the chain in the − state is $p_-(c_0) = 1 - p_+(c_0)$. In what follows, we approximate the probability distribution $P(\tilde{h})$ for either Cartesian component of $\tilde{\mathbf{h}}(\tilde{s})$ in the tranparent state by a Gaussian distribution

$$P(\tilde{h}_\alpha) = \frac{1}{\sqrt{2\pi}R_e} e^{-\tilde{h}_\alpha^2/2R_e^2}. \tag{30}$$

This yields corresponding probabilities

$$p_\pm(c_0) = \Phi\left(\pm\frac{c_0}{R_e}\right), \tag{31}$$

where

$$\Phi(x) \equiv \int_{-x}^{\infty} \frac{dy}{\sqrt{2\pi}} e^{-y^2/2} \tag{32}$$

is a normal distribution function.

The increase in the single-chain fluctuation free energy of the medium chain due to the presence of an uncrossable test chain, relative to that in the transparent state, is given for a chain trapped in either the + or − configuration by a function

$$a_\pm(c) = -T \ln \Phi\left(\pm\frac{c}{R_e}\right) \tag{33}$$

of the separation $c = c_0 - h_1$ given in Eq. (27). The magnitude of the average force exerted between the test rod and the specified medium chain, in either possible topological state, is given by the derivative

$$\langle f_\pm \rangle = \left.\frac{\partial a_\pm}{dh_1}\right|_{c_0}, \tag{34}$$

where $\langle \cdots \rangle$ is used here to indicate an average over thermal fluctuations of the medium chain in the presence of an uncrossable test rod. The average of this force over the two possible topological states may be expressed as the corresponding derivative

$$\langle f \rangle = \left. \frac{\partial a}{\partial h_1} \right|_{c_0} \tag{35}$$

of an average binary interaction free energy

$$a(c,c_0) \equiv p_-(c_0)a_-(c) + p_+(c_0)a_+(c). \tag{36}$$

Note that, because the topological state of the network cannot change as a result of the displacement of the test chain, the probabilities $p_\pm(c_0)$ depend only upon the initial distance of closest approach c_0 between the test rod and the preferred tube contour of the medium chain, while the free energies $a_\pm(c)$ depend upon the corresponding distance c obtained after displacement of the test chain.

The total effective potential experienced by the test rod is obtained in the BCA by averaging the binary interaction free energy $a(c,c_0)$ over all possible orientations and positions of the preferred tube contours of nearby medium chains. This average may be expressed as the integral

$$\Gamma_{conf}(h) = L \int_{-\infty}^{\infty} dc_0 \int d\tilde{\mathbf{u}}\, \rho(\tilde{\mathbf{u}},c_0) a(c,c_0), \tag{37}$$

where $\tilde{\mathbf{u}}$ is integrated over half of the unit circle, and where $\rho(\tilde{\mathbf{u}},c_0)d\tilde{\mathbf{u}}dc_0$ is the average number of medium chains per unit length of the test chain with tube contour orientations that lie within an infinitesimal range of solid angles $d\tilde{\mathbf{u}}$ and values of c_0 within an infinitesimal range dc_0. If the tube contours of the medium chains are assumed to have random positions and orientations, then

$$\rho(\tilde{\mathbf{u}},c_0) = \frac{1}{2\pi} \rho \sin(\theta), \tag{38}$$

where $\cos(\theta) \equiv \tilde{\mathbf{u}} \cdot \mathbf{u}$, and where ρ is the total density of contour length per volume.

Using Eqs. (37) and (38), the free energy difference

$$\Delta\Gamma_{conf}(h) \equiv \Gamma_{conf}(h) - \Gamma_{conf}(0) \tag{39}$$

arising from a transverse displacement h may be expressed as a function of the form

$$\Delta\Gamma_{conf}(h) = LT\rho R_e F\left(\frac{h}{R_e}\right), \tag{40}$$

where

$$F(x) \equiv -\frac{1}{8}\int_{-\infty}^{\infty} dy_0 \int_0^{2\pi} d\phi \left\{ \Phi(-y_0) \ln\left(\frac{\Phi(-y)}{\Phi(-y_0)}\right) + \Phi(y_0)\ln\left(\frac{\Phi(y)}{\Phi(y_0)}\right)\right\}, \tag{41}$$

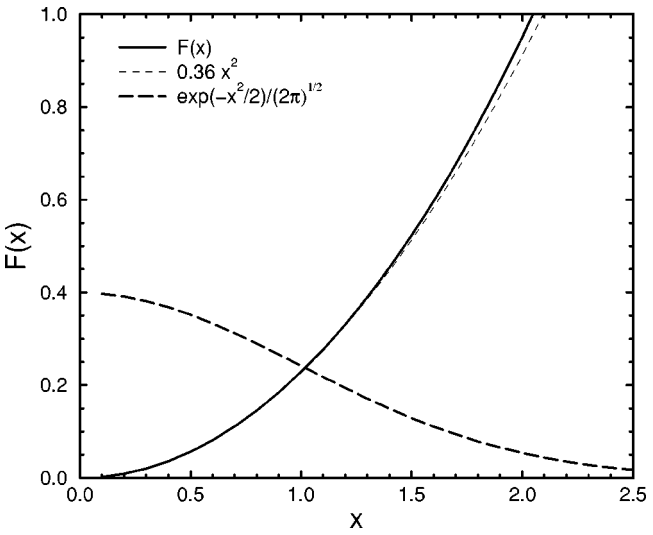

FIG. 3. The function $F(x)$ defined in Eq. (41) (solid line), the harmonic approximation $F(x) \simeq 0.36x^2$ of Eq. (42) (long-dashed line), and the Gaussian distribution $P(h/R_e)$ (short-dashed line).

in which $y \equiv y_0 - \cos(\phi)x$. In the above, $x = h/R_e$, $y_0 = c_0/R_e$, $y = c/R_e$, and $\cos(\phi) = h_1/h$.

The function $F(x)$ has been calculated by numerically evaluating the integrals in Eq. (41), and is shown in Fig. 3. The function is well approximated over the physically relevant range of displacments $x \lesssim 1$ by a parabola

$$F(x) \simeq \alpha x^2 \tag{42}$$

with $\alpha \simeq 0.36$. The harmonic approximation that we used for the effective potential of the medium chains (which was originally chosen for mathematical simplicity) is thus found to be surprisingly close to the shape predicted by the BCA.

B. Confinement of a semiflexible chain

An analogous calculation is given in Appendix B for the effective potential $\Gamma(\overline{\langle h \rangle})$ experienced by a semiflexible test chain subjected to a specified external force. The calculation differs from that given above for a rigid test rod in that we treat the test and medium chain on a more equal footing, by allowing the test chain also to undergo thermal fluctuations within a tube.

It is found that the only effect of this change is to increase the characteristic width of the potential found above by a factor of $\sqrt{2}$, without changing its form: The calculated effective potential for a semiflexible test chain is

$$\Delta\Gamma_{conf}(h) = LT\rho R_e F\left(\frac{h}{\sqrt{2}R_e}\right), \tag{43}$$

where $h \equiv |\overline{\langle \mathbf{h} \rangle}|$, and where $F(x)$ is the function defined in Eq. (41). If $F(x)$ is again approximated by Eq. (42), then one obtains a confinement potential

$$\Delta\Gamma_{conf}(h) \simeq \tfrac{1}{2} L(\alpha T\rho/R_e)|\overline{\langle \mathbf{h} \rangle}|^2 \tag{44}$$

and a corresponding approximation for $\gamma(q)$ as

$$\gamma(q) = \alpha T\rho/R_e . \tag{45}$$

The net effect of taking into account the semiflexibility of the test chain is thus to decrease the q-independent effective spring constant γ by a factor of 2, relative to that obtained for a rigid test rod.

This softening of the effective potential for a semiflexible chain is a result of the fact that in Appendix B the test chain has been allowed to bend so as to avoid nearby medium chains, as well as the reverse. The observation that the width of the effective potential depends upon the flexibility of the test chain, as well as that of the medium chains, is consistent with the observation that the tube diameter would shrink to zero in the case of an infinitely long rigid test rod in a network of infinite rigid rods, but would remain nonzero for either a rigid test rod in a network of semiflexible chains or a semiflexible test chain in a network of rigid rods.

C. Self-consistent solution

A self-consistent approximation for R_e may be obtained by substituting Eq. (45) for $\gamma(q)$ into Eq. (7) for R_e. This yields an integral equation for R_e as

$$R_e^2 = \int \frac{dq}{2\pi} \frac{1}{L_p q^4 + \alpha\rho/R_e}. \tag{46}$$

By analytically completing the above integral, solving for R_e, and using the resulting value for $\gamma(q)$ in Eq. (10) for L_e, one obtains

$$R_e = L_p(4\alpha\rho L_p^2)^{-3/5},$$

$$L_e = L_p\left(\frac{\alpha}{8}\rho L_p^2\right)^{-2/5}, \tag{47}$$

giving

$$R_e \simeq 0.80\rho^{-3/5}L_p^{-1/5}, \tag{48}$$

$$G \simeq 0.40T\rho^{7/5}L_p^{-1/5} \tag{49}$$

for $\alpha = 0.36$. As noted in Sec. II, the exponents in the above are the same as those obtained by Semenov [3] by a simple geometrical argument. Here, however, we have also obtained estimates of the prefactors.

V. EFFECTIVE MEDIUM APPROXIMATION

In the effective medium approximation, we treat the network surrounding the test chain as an elastic continuum with a shear modulus equal to the plateau modulus of the solution, and assume that the test chain rigidly follows any displacment of this medium. To calculate $\gamma(q)$, we consider a situation in which the test chain is subjected to an external force $\mathbf{f}(s)$ that contains only a single nonzero Fourier amplitude $\mathbf{f}(q)$, and use continuum mechanics to calculate the resulting displacement amplitude $\mathbf{h}(q)$, setting $\mathbf{f}(q) = \gamma(q)\mathbf{h}(q)$ to define $\gamma(q)$.

A. Continuum mechanics

The three-dimensional (3D) displacement of the elastic medium is described by a vector field $\mathbf{U}(\mathbf{r})$, where $\mathbf{r}$ is a 3D position. We assume that the test chain is rigidly embedded in the medium along the line $\mathbf{r}(s) = s\mathbf{u}$, so that the displacement $\mathbf{h}(s)$ of the chain is given (in the linear response regime) by the value

$$\mathbf{h}(s) \equiv \mathbf{U}(s\mathbf{u}) \tag{50}$$

of the 3D displacement field evaluated along this line. The elastic energy of the isotropic medium may be expressed in the standard form

$$E = \tfrac{1}{2}\int d\mathbf{r}\left\{ 2G\sum_{ij} (\epsilon_{ij})^2 + (B - \tfrac{2}{3}G)\left(\sum_i \epsilon_{ii}\right)^2\right\}, \tag{51}$$

where $\epsilon_{ij} = (\partial U_j/\partial r_i + \partial U_i/\partial r_j)$ is the strain tensor, and G and B are the shear modulus and isotropic compression modulus of the medium, respectively. In the present context, G and B are given by the plateau values of the shear modulus and the osmotic compression modulus of the entangled solution, as measured when the solution is subjected to a deformation with a characteristic frequency lying within the plateau regime of $G'(\omega)$, where the stress is dominated by the curvature stress. In the molecular theory presented in Ref. [11], it was found that the curvature stress is described by a traceless tensor, implying that the curvature contributions to B vanishes identically. In the limit of infinitely thin chains, where excluded volume contributions to B are also negligible, we may thus set $B = 0$.

The 3D Fourier transform of the displacement field induced by an arbitrary force distribution $\mathbf{F}(\mathbf{r})$ exerted on the continuum is given, for $B = 0$, by

$$\mathbf{U}(\mathbf{k}) = \frac{1}{G|\mathbf{k}|^2}\{\boldsymbol{\delta} - \tfrac{1}{4}\hat{\mathbf{k}}\times\hat{\mathbf{k}}\}\cdot\mathbf{F}(\mathbf{k}), \tag{52}$$

where $\mathbf{U}(\mathbf{k})$ and $\mathbf{F}(\mathbf{k})$ are 3D Fourier components of $\mathbf{U}(\mathbf{r})$ and $\mathbf{F}(\mathbf{r})$, and $\hat{\mathbf{k}} \equiv \mathbf{k}/|\mathbf{k}|$. The corresponding result for the 1D Fourier transform $\mathbf{h}(q)$ of the chain displacement $\mathbf{h}(s) \equiv \mathbf{U}(s\mathbf{u})$ is given by the 2D Fourier integral

$$\mathbf{h}(q) = \int \frac{d^2k_\perp}{(2\pi)^2} \frac{1}{G|\mathbf{k}|^2}\{\boldsymbol{\delta} - \tfrac{1}{4}\hat{\mathbf{k}}\times\hat{\mathbf{k}}\}\cdot\mathbf{F}(\mathbf{k}), \tag{53}$$

in which $\mathbf{k} \equiv \mathbf{u}q + \mathbf{k}_\perp$ and $\hat{\mathbf{k}} \equiv \mathbf{k}/|\mathbf{k}|$, where $\mathbf{k}_\perp \cdot \mathbf{u} = 0$.

B. Force distribution

In the above, we have calculated the displacement along the axis $\mathbf{r} = \mathbf{u}s$ for an elastic continuum subjected to an arbitrary force distribution $\mathbf{F}(\mathbf{r})$. The only choice for the force distribution $\mathbf{F}(\mathbf{r})$ that is consistent with our naive picture of the test chain as an infinitely thin thread embedded in the medium is one in which the force is transmitted to the medium at points lying exactly on line $\mathbf{r} = s\mathbf{u}$, giving

$$\mathbf{F}(\mathbf{r}) = \int ds\, \delta(\mathbf{r} - \mathbf{u}s) \times \mathbf{f}_{conf}(s), \tag{54}$$

or, equivalently, $\mathbf{F}(\mathbf{k}) = (2\pi)^2 \mathbf{f}_{conf}(\mathbf{k}\cdot\mathbf{u})$. It is straightforward to confirm, however, that the use of such a singular line distribution in Eq. (53) would lead to a logarithmically divergent value for $\mathbf{h}(q)$. In real space, the displacement field $\mathbf{U}(\mathbf{r})$ induced by a line distribution of force that oscillates with wave number q along the test chain may be shown to vary logarithmically with the distance r from the test chain for $qr \lesssim 1$ and to decay exponentially for $qr \gtrsim 1$, and thus (like the electrostatic potential induced by a line charge) to diverge along the axis $\mathbf{r} = s\mathbf{u}$. To control this short-wavelength divergence, we are forced to introduce a cutoff length, below which the continuum approximation is assumed to break down. By removing short-wavelength components of $\mathbf{F}(\mathbf{k})$, such a cutoff will effectively smear the applied force over a region of nonzero radius around the test chain.

Physical considerations suggest that this cutoff length should be taken to be of order the entanglement length L_e. Forces exerted on a chain may be transmitted along its backbone over distances of order the distance L_e between collisions with other chains or (equivalently) the walls of its tube, indicating that the network cannot be treated as a continuum over length scales less than L_e. A more detailed consideration of how the external force exerted on the test chain is distributed via binary collisions to the surrounding network also suggests a possible reinterpretation of the continuum theory, which will be developed further in the elastic network model of Sec. VI: The forces exerted by a test chain upon its surroundings are first transmitted by binary collsions to a relatively small set of chains, referred to here as ''primary'' medium chains, whose tube contours happen to pass within a distance of order R_e of the test chain. The forces exerted on the primary medium chains by the test chain are balanced by forces exerted upon the primary chains by ''secondary'' medium chains, which form the walls of the tubes that confine the primary chains. The net effect of collisions between primary and secondary chains is mimicked in the binary collision approximation by the introduction of a confinement potential for each of the primary medium chains. The forces exerted between primary and secondary medium chains (or, equivalently, between primary medium chains and the walls of their tubes) are distributed along the contour of each primary medium chain over distances of order L_e away from the point of interaction with the test chain. The divergence in the effective medium theory may thus be removed in a natural way if we reinterpret the force $\mathbf{F}(\mathbf{r})$ as an ensemble average of the forces exerted between primary and secondary medium chains, rather than as an average of the force exerted by the test chain upon primary chains. In the EMA, this reinterpretation of $\mathbf{F}(\mathbf{r})$ is introduced merely as a way of regularizing the continuum mechanical calculation, in which I continue to assume that the test chain rigidly follows the calculated displacement $\mathbf{U}(\mathbf{r})$ of the continuum. In the elastic network approximation of of Sec. VI, I will take this reinterpretation more seriously, by interpreting the continuum displacement $\mathbf{U}(\mathbf{r})$ as an average displacement of the secondary medium chains, and thus allowing the displacement of the test chain to differ from that of the continuum.

In Appendix B, I present an approximate calculation of the distribution of forces exerted by the primary medium chains upon secondary medium chains that confine them, based on the above ideas. I obtain an approximate force distribution of the form

$$\mathbf{F}(\mathbf{r}) = \int ds \chi(\mathbf{r} - s\mathbf{u}) \times \mathbf{f}_{conf}(s), \tag{55}$$

in which $\chi(\mathbf{r})$ is a distribution function (specified below) that drops off rapidly for $|\mathbf{r}| \gtrsim L_e$, which serves to redistribute the force $\mathbf{f}(s)$ over a region of radius L_e around the test chain, and which satisfies the normalization condition $\int d\mathbf{r}\chi(\mathbf{r}) = 1$. The approximation introduced in Appendix B yields a distribution function with a 3D Fourier transform

$$\chi(\mathbf{k}) = \int \frac{d\tilde{\mathbf{u}}}{2\pi} \frac{\gamma_e}{TL_p(\mathbf{k}\cdot\tilde{\mathbf{u}})^4 + \gamma_e}, \tag{56}$$

in which $\tilde{\mathbf{u}}$ is a medium chain orientation that varies over half of the unit sphere, and γ_e is an approximation for $\gamma(q)$ as a q-independent constant $\gamma_e = TL_p q_e^4$, where $q_e \equiv 2^{-3/2}/L_e$.

Any force of the form given in Eq. (55), when substituted in Eq. (53), will yield a displacement of the form $\mathbf{h}(q) = \mathbf{f}(q)/\gamma(q)$, where

$$\gamma(q) = G/H(q) \tag{57}$$

and where

$$H(q) = \int \frac{d^2k_\perp}{(2\pi)^2} \frac{\chi(\mathbf{k})}{|\mathbf{k}|^2} \frac{|\mathbf{k}|^2 - \frac{1}{8}|\mathbf{k}_\perp|^2}{|\mathbf{k}|^2} \tag{58}$$

is a dimensionless compliance, in which $\chi(\mathbf{k})$ is the 3D transform of $\chi(\mathbf{r})$. A qualitative understanding of the q dependence of $H(q)$ may be obtained by replacing $\chi(\mathbf{k})$ by a sharp cutoff that suppresses all wave vectors with $|\mathbf{k}| > 1/L_e$. This yields limiting behaviors

$$H(q) \simeq \begin{cases} \dfrac{-7/8}{2\pi} \ln(qL_e), & qL_e \ll 1 \\ 0, & qL_e \gg 1. \end{cases} \tag{59}$$

The logarithmic divergence of $H(q)$ in the limit of small q, which is generic, is a reflection of the fact that the displacement field induced by a force of wave number q varies logarithmically with distance r from the test chain for all $L_e \lesssim r \lesssim q^{-1}$, and thus extends to points far from the test chain. Use of approximation (56) for $\chi(\mathbf{k})$ in Eq. (58) results in a dimensionless compliance $H(q)$ that is well approximated for all $qL_e \lesssim 25$ by the function

$$H(q) \simeq \frac{7/8}{4\pi} \ln\left(\frac{1 + (q/q_e)^2}{(q/q_e)^2} \right) + \frac{0.141}{1 + (q/q_e)^{1.5}/2}, \tag{60}$$

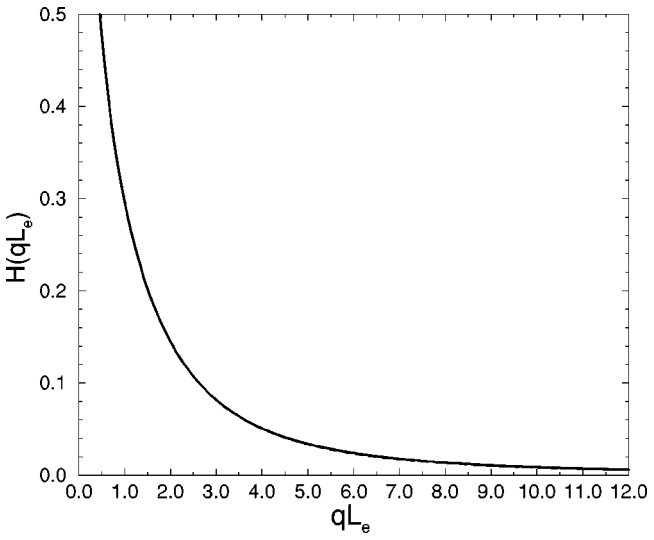

FIG. 4. Function H defined by Eqs. (56) and (58) (solid line), plotted as a function of $qL_e=2^{3/2}q/q_e$, and the analytic approximation given in Eq. (60) (dashed line).

as shown in Fig. 4, which has the low and high q limiting behaviors given in Eq. (59).

C. Self-consistent solution

The EMA, with any choice for the distribution function χ, may be made self-consistent by using Eq. (57) for $\gamma(q)$ (which is the result of a continuum mechanical calculation) in Eqs. (9) and (10) for G (which are the results of a molecular theory), and then requiring that the prediction of the molecular theory for G agree with the value assumed for the surrounding medium. This yields an integral equation for G as

$$G=\frac{7\rho T}{5}\int\frac{dq}{2\pi}\frac{G/H(q)}{TL_pq^4+G/H(q)}. \tag{61}$$

If $H(q)$ may be expressed as a function $H(q)=\hat{H}(qL_e)$ of $x\equiv qL_e$, then Eq. (61) may be nondimensionalized to obtain the integral equation

$$1=\int\frac{dx}{2\pi}\left[\frac{5}{7}\frac{L_p}{\rho L_e^3}\hat{H}(x)x^4+1\right]^{-1}. \tag{62}$$

The solution of Eq. (62) yields a constant numerical value for the dimensionless ratio $L_p/(\rho L_e^3)$, thus giving an entanglement length

$$L_e\propto L_p^{1/3}\rho^{-1/3}, \tag{63}$$

with a numerical prefactor whose value depends upon the exact functional form used for $\hat{H}(x)$. By using the resulting value for L_e in Eq. (9) for G and Eq. (7) for R_e, we obtain expressions for G and R_e that generically vary with ρ and L_p with the power law exponents given in Eq. (21). The numerical prefactors depend weakly upon the exact form used for $H(q)$. Using approximation (60) for $H(q)$ and numerically solving Eq. (62) yields

$$R_e\simeq 0.42\rho^{-1/2}, \tag{64}$$

$$G\simeq 0.82T\rho^{4/3}L_p^{-1/3} \tag{65}$$

for the tube radius and modulus.

VI. ELASTIC NETWORK APPROXIMATION

The elastic network model is an attempt to combine the virtues and avoid the most obvious defects of the binary collision and effective medium approaches. The BCA yields a rather detailed description of the motion of a test chain in a partially frozen local environment. The effective medium approximation allows the environment of a test chain to deform like an elastic continuum, but then unrealistically forces the test chain to rigidly follow the surrounding continuum. A better model should allow both for the elastic deformation of the surrounding network (which is found to dominate the displacement at sufficiently small q) and for a local displacement of the test chain relative to that of neighboring chains.

In the ENA, the average displacement of a test chain in response to an external force $\mathbf{f}$ is expressed as the sum

$$\overline{\langle\mathbf{h}(q)\rangle}=\overline{\langle\mathbf{h}_{local}(q)\rangle}+\overline{\langle\mathbf{h}_{coll}(q)\rangle} \tag{66}$$

of a collective elastic displacement $\overline{\langle\mathbf{h}_{coll}(q)\rangle}$ of the environment of the test chain, plus a local displacement $\overline{\langle\mathbf{h}_{local}(q)\rangle}$ of the test chain relative to that of its environment. The collective displacement $\overline{\langle\mathbf{h}_{coll}(q)\rangle}$ is understood in the ENA to represent an average displacement of the preferred tube contours of the primary medium chains. Correspondingly, the local displacement is understood to represent a displacement of the test chain relative to that of the preferred tube contours of the primary medium chains. This local displacement may be approximated using the results of the BCA, which describes the displacement of the test chain in an environment in which the preferred tube contours of the primary medium chains remain frozen when a force is exerted on the test chain. We thus set

$$\overline{\langle\mathbf{h}_{local}(q)\rangle}=\mathbf{f}_{conf}(q)/\gamma_{BCA}(q), \tag{67}$$

where $\gamma_{BCA}(q)\equiv\alpha\rho/R_e$ is the BCA approximation for $\gamma(q)$ given in Eq. (45). Correspondingly, the collective displacement of the preferred tube contours of primary medium chains, which reflect only the interactions between primary and secondary medium chains, may be treated in an effective medium approximation, in which the force $\mathbf{F}(\mathbf{r})$ exerted on the medium is properly understood to represent an average of the force exerted by primary medium chains upon the secondary chains that confine them. We thus set

$$\overline{\langle\mathbf{h}_{coll}(q)\rangle}=\mathbf{f}_{conf}(q)/\gamma_{EMA}(q), \tag{68}$$

where $\gamma_{EMA}(q)=G/H(q)$ is the EMA approximation for $\gamma(q)$ given in Eq. (57), which was calculated using a distri-

bution of forces appropriate to this interpretation. The ENA thus uses the continuum approximation only to describe elastic relaxation of the preferred tube contours of the primary medium chains (rather than that of the test chain itself), while using the BCA to describe the additional local displacement of the test chain.

Adding these two contributions yields a total displacement of the form $\mathbf{h}(q)=\mathbf{f}_{conf}(q)/\gamma(q)$, with a total compliance

$$\frac{1}{\gamma(q)}=\frac{1}{\gamma_{EMA}(q)}+\frac{1}{\gamma_{BCA}(q)} \tag{69}$$

in which the two mechanisms of displacement act in parallel. Using explicit results for $\gamma_{EMA}(q)$ and $\gamma_{BCA}(q)$ yields

$$\frac{1}{\gamma(q)}=\frac{H(q)}{G}+\frac{R_e}{\alpha\rho}. \tag{70}$$

Because $H(q)$ diverges logarithmically for $qL_e \ll 1$, the calculated compliance $1/\gamma(q)$ is dominated in the low-q limit by the first term, representing the elastic deformation of the network. In this limit, the elastic deformation is spread over a distance $q^{-1} \gg 1$, and so the continuum approximation is also expected to become increasingly accurate. In the opposite short-wavelength limit $qL_e \gg 1$, $H(q)$ vanishes, and the compliance is instead dominated by the second term, representing the local displacement of the test chain.

To make the ENA self-consistent, we substitute Eq. (70) for $\gamma(q)$ into Eq. (7) for R_e and Eqs. (9) and (10) for G, and require that the calculated values of R_e and G be consistent with those assumed for the medium chains in the calculation of $\gamma_{BCA}(q)$, and for the continuum in the calculation of $\gamma_{EMA}(q)$, respectively. The resulting pair of coupled integral equations must be solved numerically, and does not yield a simple power law dependence for R_e or G on ρ and L_p.

Predictions of the BCA, EMA, and ENA for the ratios R_e/L_p and L_e/L_p are shown in Fig. 5 as functions of the dimensionless concentration ρL_p^2. Because the ENA allows local and collective displacement mechanisms to act in parallel, the ENA always yields the largest of the three values for R_e or L_e. The ENA results converge to the EMA results at very high values of ρL_p^2, but the BCA predictions for R_e and L_e remain larger than the asymptotically correct EMA values until rather large values of ρL_p^2. The crossover of the BCA and EMA predictions for L_e occurs at much higher values of ρL_p^2 than the crossover for R_e, because Eq. (10) for L_e is less sensitive to the logarithmic low-q softening of $\gamma(q)$ than is Eq. (7) for R_e. At values of $\rho L_p^2 \sim 10^4$ typical of the *F*-actin solutions discussed below, L_e is about one order of magnitude larger than R_e and one order of magnitude smaller than L_p.

The ENA predictions for the ratio L_e/L_p do not drop to values significantly below unity until rather large values of ρL_p^2, e.g., $L_e/L_p \simeq 0.5$ for $\rho L_p^2 = 10^2$. This suggests that a well defined tightly entangled regime, with $L_e \ll L_p$, can occur only for very large values of ρL_p^2. If so, there must exist a very wide crossover between the regions of validity of the

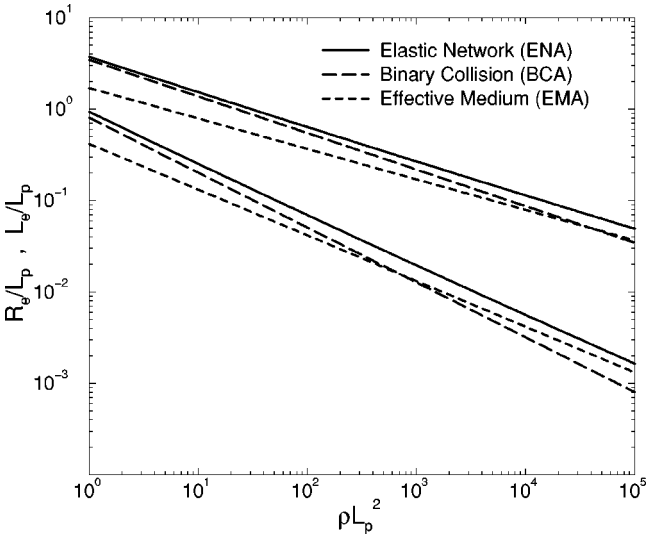

FIG. 5. Predicted values of the dimensionless tube radius R_e/L_p and entanglement length L_e/L_p vs dimensionless concentration ρL_p^2. The upper three lines are values of L_e/L_p and the lower three are values of R_e/L_p, as predicted by the elastic network model (solid line), the binary collision approximation (long-dashed line), and the effective medium approximation (short-dashed line).

original tube model of flexible chains, which is strictly valid only for $L_p \ll L_e$, and that of the present model, which is valid for $L_e \ll L_p$. Much of the available data on isotropic solutions of long wormlike chains on systems with values of L_p/d smaller than that found for *F*-actin could fall into this crossover regime. The present model is expected to underestimate L_e/L_p for small values of ρL_p^2, since the weak concentration dependence of $L_e \propto \rho^{-(0.4-0.5)}$ obtained here must eventually cross over to the steeper $L_e \propto \rho^{-1.3}$ or $G \propto \rho^{2.3}$ dependence that is found for semidilute solutions of flexible chains.

One weakness shared by the ENA and EMA is that the predictions of both approximations depend upon the value chosen for a cutoff length used to regularize the continuum mechanical description of the strain field around a test chain. I have relied here upon a physical picture of the mechanism of force transmission over short distances within a network that suggests a cutoff length of order L_e, and, in Appendix C, have tried to translate this picture into a well defined regularization scheme. A very different argument for the magnitude of such a cutoff length has been given by Maggs, in a discussion of the deformation induced by displacements of a very small bead embedded in a network of semiflexible chains [8], who argued for the breakdown of continuum elasticity below a larger cutoff length of order $\sqrt{L_e L_p}$. For the *F*-actin solutions considered below, for which I find $L_p \sim 10 L_e$, Maggs's result would suggest the use of a cutoff length several times larger than that used above, with a weaker dependence on concentration. Without trying here to resolve the discrepancy between these estimates, I will note that the predictions of the ENA do not depend very strongly on the choice of a value for the cutoff length, for two reasons. First, the quantity $\gamma_{EMA}(q)=G/H(q)$ that is obtained from continuum mechanics depends only logarithmically on

the cutoff length, as shown in Eq. (59), where L_e appears within a logarithm. The EMA prediction of a power law $L_e \propto \rho^{-1/3}$ is a consequence of the algebraic dependence of G upon L_e, rather than the logarithmic dependence of $H(q)$ upon L_e, and would be modified only by logarithmic corrections if a cutoff length proportional to $\sqrt{L_e L_p}$ were used in place of one proportional to L_e. Second, the use of a larger cutoff length in the calculation of $\gamma_{EMA}(q)$ would decrease the collective contribution to the total ENA compliance $1/\gamma(q)$ in Eq. (70), but cannot cause the ENA compliance to drop below that obtained from the BCA alone. For parameters typical of *F*-actin solutions at experimentally relevant concentrations (discussed below), it is found that the BCA and ENA predictions for L_e differ by only about a factor of 2, which further limits the sensitivity of the ENA predictions for *F*-actin to increases in the choice of cutoff length.

VII. *F*-ACTIN SOLUTIONS

Solutions of actin protein filaments (*F*-actin) are so far unique in that (i) the filaments are sufficiently long, stiff, and thin to be able to form isotropic solutions with $\rho L_p^2 \simeq 10^4$ and $L \sim L_p \simeq 10 L_e$, placing them well within the tightly entangled concentration regime, and (ii) independent measurements are available of the persistence length, the tube diameter (both measured by fluoresence microscopy), and the plateau modulus (measured by both mechanical and optical rheometry). That these solutions are tightly entangled is graphically confirmed by fluoresence micrographs that show confinement of filaments many micrometers long, with persistence lengths of order 10 μm, to tubelike regions that are only a few tenths of a micrometer across [21,22]. In this section, theoretical predictions are compared to experimental measurements of both R_e and G in *F*-actin solutions.

A. Persistence length and diffusivity

I begin by reviewing measurements of the persistence length and tangential diffusivity by fluoresence microscopy, which are needed as inputs to the theory.

The persistence length of *F*-actin has been measured by several groups [23–25] by analyzing observations of the Brownian fluctuations of fluorescently labeled filaments in unentangled solutions [23–25]. A value of $L_p = 17 \pm 1$ μm has been consistently obtained from observations of filaments that are stabilized against continuous polymerization and depolymerization by addition of fluorescently labeled phalloidin, which allows the filaments to be diluted below the critical polymerization concentration for visualization. Isambert *et al.* [25] report a persistence length of $L_p = 18 \pm 1$ μm for phalloidin-stabilized actin, in agreement with earlier studies [23,24], but find a lower value of $L_p = 9 \pm 1$ μm for rhodamine-labeled actin filaments that are not stabilized by phalloidin, which were visualized very near the critical polymerization concentration in order to produce a solution containing a few long filaments diluted by a larger concentration of monomeric actin. It not yet clear whether the properties of labeled but unstabilized actin or those of actin stabilized with labeled phalloidin are more representative of the properties of unlabeled, unstabilized actin of the sort used in most rheological studies. Except where otherwise noted, we will assume a persistence length of 17 μm in what follows.

Käs *et al.* [21,22] have also used fluoresence microscopy to measure the tangential diffusivity D_{rep} of entangled actin filaments as a function of contour length. They find that the dependence of D_{rep} on chain length, for chains of length 7–60 μm, is roughly consistent with an Einstein relation of the form $D_{rep} = T/(\zeta L)$, with a friction coefficient per unit length of $\zeta = 0.1 - 0.2$ dyne s cm^{-2} that shows no measurable dependence on concentration.

The values of ζ needed to describe Kas *et al.*'s observations of reptation are significantly larger than those obtained by calculating the hydrodynamic drag associated with dragging a cylindrical fiber tangentially through an aqueous solvent. The friction coefficient of $\zeta \simeq 0.16$ dyne s cm^{-2} obtained from measurements of D_{rep} for the two shortest fibers of $L = 6.9$ μm and 11.2 μm in [22] corresponds to the use in Eq. (9) of [12] of an effective solvent viscosity $\eta_s = 0.08$ dyne s cm^{-2}, i.e., eight times the viscosity of water. This sluggish tangential diffusion could in principle be due to either attractive or repulsive interactions between chains, i.e., diffusion could be slowed either by having the chains stick weakly to one another or by jamming of chains against one another. The effect of steric jamming of rigid rods upon tangential diffusion was considered theoretically by Edwards and Evans [33], who showed that the effect could become important at concentrations near the isotropic-nematic transition concentration ρ_{IN}, but were unable to give a reliable quantitative treatment. Observations of entangled *F*-actin filaments by Kas *et al.* were carried out at concentrations close to ρ_{IN}.

Measurements of self-diffusivity of the rodlike polymer poly(γ-benzyl glutamate) (PBG) in concentrated solutions by Bu *et al.* [34], using fluorescence photobleaching recovery, have shown that the tangential self-diffusivity of PBG decreases significantly at concentrations approaching ρ_{IN}. Bu *et al.* find that the ratio D/D_0 of the diffusivity D to the value D_0 obtained in dilute solution, for samples with several different molecular weights, appears to be a function of the ratio ρ/ρ_{IN} alone, and find a value of $D/D_0 \sim 0.1$ near the *I*-*N* transition. Complete suppression of the diffusion of a rodlike polymer in the two directions perpendicular to the chain, due to the formation of a cage of surrounding molecules, in the absence of any reduction in tangential diffusivity, would by itself reduce D/D_0 to about 1/2. (This value reflects the fact that the tangential diffusivity of a thin rod in dilute solution is about twice its diffusivity in either perpendicular direction.) The observation of values of D/D_0 substantially less than 1/2 thus implies that tangential, as well as perpendicular, diffusivity must be substantially decreased in concentrated solutions. Both the observed scaling of D/D_0 with ρ/ρ_{IN} and the fact the PBG molecules in pyridine are believed to interact as simple hard rods suggest that decrease of tangential diffusivity in PBG solutions is a result of steric jamming. This, in turn, suggests jamming as the more likely of the two possible causes of the low tangential diffusivity in *F*-actin.

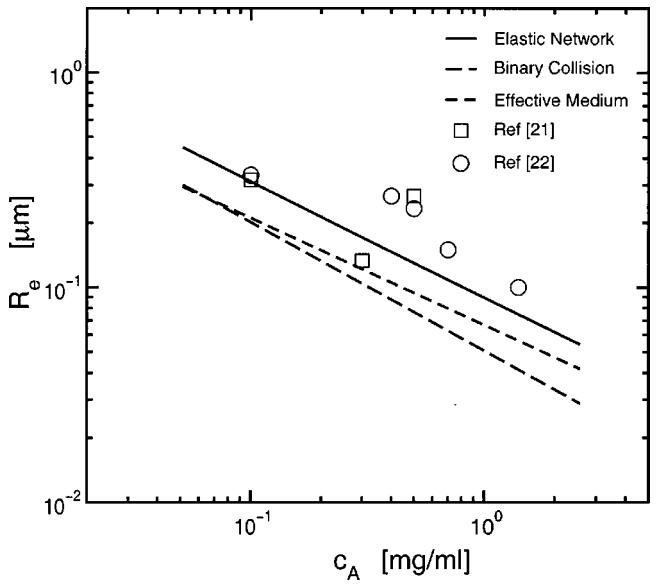

FIG. 6. Tube radius R_e vs actin concentration c_A. Results of Kas *et al.* [21,22] for the tube radius in *F*-actin solutions, obtained by reanalysis of fluoresence microscopy data originally reported in Ref. [21] (open squares) and Ref. [22] (open circles), compared to predictions of the elastic network (solid line), binary collision (long-dashed line), and effective medium (short-dashed line) approximations.

The contour length density of *F*-actin for a solution with an actin concentration of $c_A = 1$ mg/ml, which is typical of the measurements considered below, is 39 μm^{-2}, based on a helical repeat unit of 360 Å containing 13 monomers with a monomer molecular weight of 42 000. This corresponds, for $L_p = 17$ μm, to a dimensionless concentration of $\rho L_p^2 = 1.1 \times 10^4$.

B. Tube radius

Käs *et al.* [21,22] have obtained a quantitative measure of the tube radius in *F*-actin solutions by visualizing fluctuations of single fluorescently labeled filaments within a tightly entangled solution of unlabeled filaments. Käs *et al.* record micrographs of single labeled filaments, taken at short intervals over a period greater than the entanglement time but much less than the reptation time, e.g., 64 micrographs taken at intervals of 0.1 s in Ref. [22]. They then graphically overlay the resulting images of the chain contour, to produce a bundle of overlapping lines that visually defines the tube. Values for the tube diameter originally reported in Refs. [21,22] were obtained by measuring the average width of the resulting bundle, averaged over the length of each filament, and over several filaments at each concentration. To facilitate comparison of these experiments to theory, J. Käs has kindly provided values for the actual standard deviation of $h(s)$, projected onto the focal plane of the microscope, calculated from the same data sets. The resulting values for the standard deviation are typically about three times smaller than the bundle diameters reported previously.

Figure 6 shows a comparison of the predictions for R_e of the three models presented in Secs. III–V to these data. The dependence of the measured values of R_e on concentration in Fig. 6 is consistent with any power law exponent in the range between the BCA prediction of $R_e \propto \rho^{-0.6}$ and the EMA prediction of $R_e \propto \rho^{-0.5}$. The quantative predictions of the ENA, which yields the largest tube diameter of the three models, are within the scatter of the data.

C. Plateau modulus

Attempts to compare predictions for the plateau modulus to experiments on *F*-actin are thus far plagued by the existence of significant discrepancies between values of G reported by several different experimental groups. Rheological measurements of *F*-actin solutions have been carried out by Janmey and co-workers [26], Pollard, Xu, Wirtz, and co-workers [27,28], and Sackmann and co-workers [30,31] (see references and discussion in [12]). Enormous discrepancies between values of $G \simeq 10^2 - 10^3$ dyn/cm^2 initially reported for the plateau modulus by Janmey and co-workers and values of $G \simeq 1 - 20$ dyn/cm^2 reported in Refs. [27,28,30,31] have apparently been resolved as the result of a collaboration and careful comparison of experimental procedures [29]. These large discrepancies have been traced to differences in sample preparation and storage conditions, and are now believed to have been the result of the spontaneous oxidation of monomers during storage, which led to the formation of cross-links between actin filaments upon polymerization [32], together with the sensitivity of the modulus to the presence of small concentrations of cross-links [12]. There remains, however, a smaller but apparently systematic discrepancy between values of $G \simeq 5 - 10$ dyn/cm^2 for $c_A = 1$ mg/ml recently reported for freshly polymerized actin by Xu *et al.* [29], and the lower values of $G \simeq 1$ dyn/cm^2 reported by Hinner *et al.* [31].

I noted in Ref. [12] that quantitative predictions of the plateau modulus obtained by using fluorescence microscopy measurements of the tube diameter to estimate L_e are in reasonable quantitative agreement with the measurements of Hinner *et al.* [31], and with earlier measurements by Ruddies *et al.* [30], but are, correspondingly, 5–10 times below the values recently reported in Refs. [26–29]. Here I give a more detailed comparison of theoretical predictions for the plateau modulus to the available rheological data, focusing on the data of Refs. [30,31], while now using predicted rather than measured values for the tube diameter.

1. Data of Hinner et al.

Figure 7 shows a comparison of theoretical predictions for the plateau modulus to measurements by Hinner *et al.* [31]. The values of the plateau modulus reported in Ref. [31] and reproduced here were obtained from the value of the storage modulus $G'(\omega)$ at the frequency for which $\tan(\delta) = G''(\omega)/G'(\omega)$ is minimum. Here, I use G_0' to denote moduli obtained by this prescription, and G to denote theoretical values predicted for a hypothetical solution of infinitely long chains. In many of the samples studied by Hinner *et al.*, the average chain length has been controlled by adding small concentrations of the capping protein gelsolin to the *F*-actin solution, which allows one to calculate a nominal

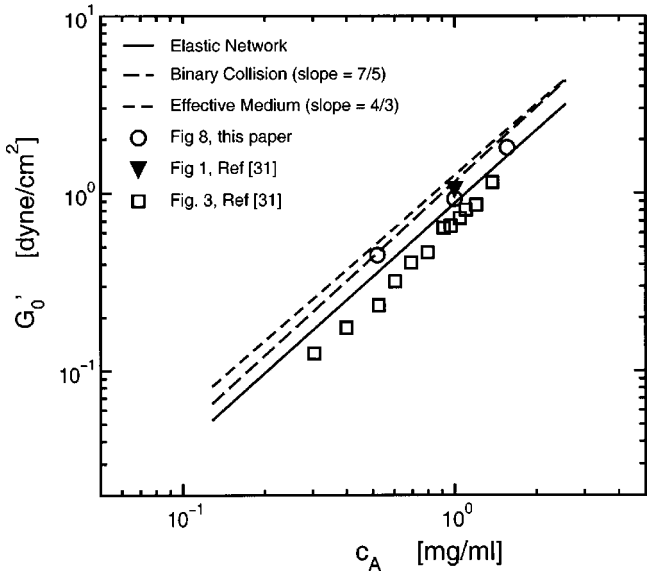

FIG. 7. Comparison of theoretical predictions for the plateau modulus G_0' vs concentration in *F*-actin solutions to results of measurements of Hinner and co-workers [31]. Predictions are given for elastic network (solid line), binary collision (long-dashed line), and effective medium approximations (short-dashed line). Open squares are the values reported in Fig. 3 of Ref. [31] for a sequence of solutions with $\overline{L}=16$ μm. The inverted triangle is the value obtained from Fig. 1 of the same paper for several solutions containing filaments of length 4 $\mu\mathrm{m}\leqslant\overline{L}\leqslant 15$ μm. Open circles are experimental values of G_0' obtained from the measurements shown in Fig. 8 below.

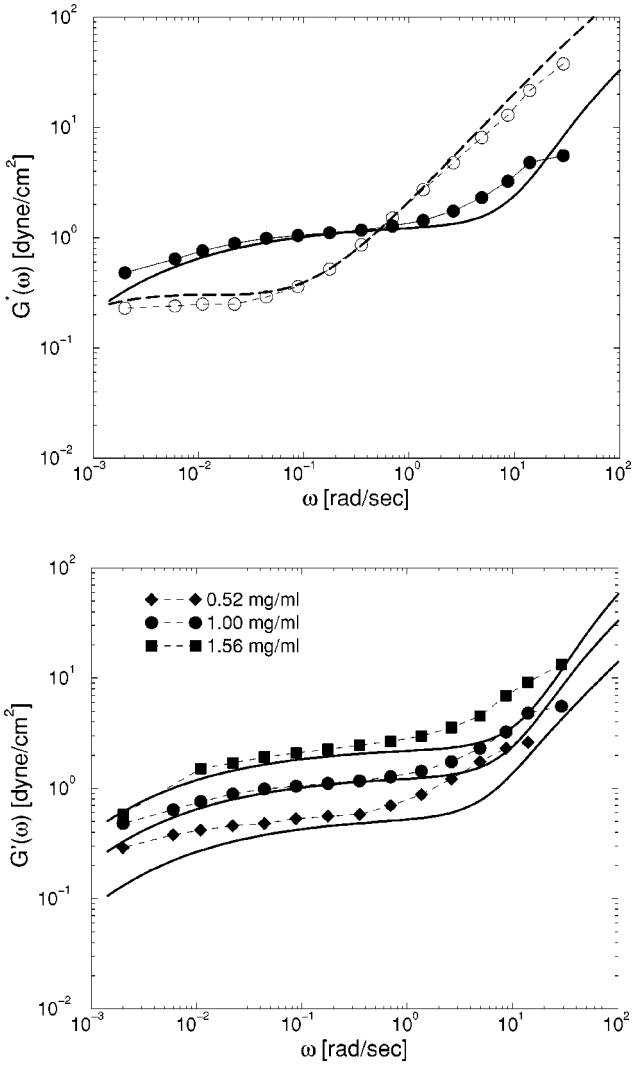

FIG. 8. Comparison of linear viscoelastic measurements of $G'(\omega)$ (closed symbols) and $G''(\omega)$ (open symbols) in *F*-actin solutions with nominal chain length of 5 μm (data provided by B. Hinner and E. Sackmann) to theoretical predictions for $G'(\omega)$ (solid lines) and $G''(\omega)$ (long-dashed line). The upper panel shows loss and storage moduli for a solution with $c_A=1.0$ mg/ml, and the lower panel shows storage moduli for three different concentrations. Short-dashed lines connecting experimental points are guides to the eye.

average chain length $\overline{L}$ under the assumption that each gelsolin caps one actin filament, and that uncapped filaments are rare. Figure 1 of Ref. [31] shows measured values of G_0', reproduced as open squares in Fig. 7, for a series of 12 solutions with actin concentrations in the range $c_A=0.3$–1.4 mg/ml and a common nominal chain length of $\overline{L}=16$ μm. This series of measurements shows a concentration dependence consistent with the power law $G_0'\propto c_A^{1.4}$ predicted by the BCA approximation and earliear scaling arguments. In Fig. 1 of the same paper, Hinner *et al.* show measurements of G_0' for a series of samples with a common actin concentration of $c_A=1.0$ mg/ml and varying nominal average chain lengths in the range 2.5 $\mu\mathrm{m}\leqslant\overline{L}\leqslant 27.5$ μm. The modulus was found to remain near a constant value $G_0'=1.05\pm 0.1$ dyn/cm^2 (shown by the inverted triangle in Fig. 7 for chains of nominal length 4 $\mu\mathrm{m}<\overline{L}<15$ μm, but to fall off rapidly for $\overline{L}<4$ μm, and to increase somewhat with increasing chain length for $\overline{L}>15$ μm. The decrease in G_0' for $\overline{L}\lesssim 4$ μm may be plausibly argued to be a result of the approach of the average chain length to the entanglement length of $L_e\simeq 2$ μm that is obtained either from the observed modulus or from the ENA. The increase in G_0' with increasing chain length for $\overline{L}>15$ μm is troubling, however, since any tube model would predict a plateau modulus that is independent of chain length in the limit of long chain lengths. The three open circles in Fig. 7 are values of G_0' obtained from the unpublished measurements of storage and loss moduli for three samples with $\overline{L}=5$ μm, which are shown in Fig. 8 and discussed in greater detail below.

The theoretical predictions for G_0' shown in Fig. 7 were obtained as follows. The BCA, EMA, and ENA were used to predict values for the plateau modulus G of a hypothetical network of infinite chains of persistence length $L_p=17$ μm. Predictions for G were used as inputs to the rheological model developed in Ref. [12] for a 1 mg/ml solution containing an exponential distribution of chain lengths with $\overline{L}=5$ μm, like those shown in Fig. 8, and G_0' was set equal to the value of $G'(\omega)$ obtained at the frequency for which $\tan(\delta)$ is minimum. This yields a modulus $G_0'=G/1.36$. Use

of the shorter reported persistence length of $L_p = 9\ \mu$m in the ENA results for $c_A = 1.0$ mg/ml in a predicted plateau modulus about 20% larger than that shown in Fig. 7, a predicted tube radius about 4% larger than that shown in Fig. 6. Changes this small would have no effect upon conclusions regarding the extent of agreement between theory and experiment. The predictions of the ENA for the plateau modulus are thus found to be in good quantitative agreement (using either value of L_p) with both the concentration dependence and absolute magnitudes of the moduli reported by Hinner and co-workers.

In Fig. 8, predictions of the rheological model of Ref. [12] for the frequency-dependendent moduli $G'(\omega)$ and $G''(\omega)$ are compared to unpublished measurements by Hinner *et al.* of $G'(\omega)$ and (for one sample) $G''(\omega)$ for three *F*-actin solutions with a common nominal chain length $\overline{L} = 5\ \mu$m. Predicted storage and loss moduli are obtained by using the ENA prediction for *G* as an input to the rheological model, and assuming an exponential distribution of chain lengths with a number-averaged chain length $\overline{L} = 5\ \mu$m. The effective solvent viscosity used in the theory has been adjusted so as to give a tangential friction coefficient $\zeta = 0.13$ P. This value was chosen to fit the data, but is within the range of values for ζ inferred by Käs *et al.* from fluoresence microscopy observations of reptation [21,22]. The theory clearly does an excellent job of predicting both the plateau moduli (with no free parameters) and the main features of the frequency dependence in these three samples. The degree of agreement between predicted and measured plateau moduli in these samples must, however, be partially fortuitious, since Hinner estimates [35] that his data are reproducible from sample to sample only to within $\pm 50\%$, consistent with the range of values seen in Fig. 7. There is a noticeable tendency, which is apparent to greater or lesser degree in all of the available rheological data for *F*-actin solutions, for the measured values of $G'(\omega)$ to begin increasing slowly with increasing ω in a range of intermediate frequencies $\omega \gtrsim 1-10$ rad/s in which the theory predicts a much flatter plateau. The roughly linear increase of the calculated $G''(\omega)$ with frequency at frequencies $\omega \gtrsim 10^{-1}$ rad/sec is a result of the tension induced in a rodlike chain subjected to a small oscillatory shear flow, which acts to oppose the oscillatory extensional drag forces exerted on the chain by such a flow. It is possible that the slow upturn in $G'(\omega)$ at intermediate frequencies, which occurs in these samples at frequencies for which $G''(\omega) > G'(\omega)$, is a reflection of an additional curvature stress induced by this tension, which was not allowed for in Ref. [12].

2. Data of Xu et al.

Agreement between the above predictions for the plateau modulus and the results of Xu *et al.* [29] is much less satisfactory. Xu *et al.* undertook a systematic study of the effects of a number of experimental factors upon the values obtained for the plateau modulus of purified *F*-actin solutions, in an attempt to identify the origins of the large discrepancies among the values published previously in the literature (see Table I of [29]). Comparison of measurements on three different commercial rheometers housed in three different laboratories showed that one of the three (the Rheometrics RFS II at Harvard) consistently yielded moduli three times larger than those obtained from the other two instruments (a Weissenberg Rheogonimeter at Johns Hopkins University and another RFS II at the University of Maryland). Much more significantly, Xu *et al.* showed that some preparation and (particularly) storage procedures yielded samples with moduli 2–3 orders of magnitude larger than those obtained for freshly polymerized actin. Xu *et al.* reported, however, that they could obtain reproducible values for the storage modulus of freshly polymerized actin. Their results for freshly polymerized actin (using the two rheometers that yield lower moduli) show a storage modulus of $G'(\omega) \simeq 5$ dyn/cm^2 at the flattest part of the plateau, near $f \simeq 0.01$ Hz, which in most samples rises slowly to $G'(\omega) \simeq 10$ dyn/cm^2 at 1 Hz. These values are roughly consistent with those obtained in earlier studies by Pollard, Schwarz, Xu, Wirtz and various co-workers, but are roughly five times higher than those obtained by Hinner *et al.*, or those predicted by the ENA. This difference appears to be larger than the sample-to-sample variation found by Xu *et al.* for fresh actin. The reason for this remaining experimental discrepancy is not known.

VIII. CONCLUSIONS

The calculations of the tube diameter and plateau modulus given above are based upon a consideration of two very different and complementary descriptions of the interactions between a chain and its surroundings in an entangled network. The binary collision approximation attempts to explicitly describe the motion of a test chain in a partially frozen environment, in which the surrounding chains are confined to static tubes, and is based upon a detailed treatment of the interactions of two nearby chains. When treated self-consistently, this approximation yields power laws $R_e \propto \rho^{-3/5}$ and $G \propto \rho^{7/5}$ for the tube diameter and modulus, consistent with the results of a simple geometrical scaling argument, and predicts numerical prefactors that cannot be obtained from such arguments. The effective medium approximation describes the collective elastic displacement of the surrounding network by treating it as an elastic continuum. This approximation yields different power laws $R_e \propto \rho^{-1/2}$ and $G \propto \rho^{4/3}$, with exponents that happen to be numerically similar to those obtained from the binary collision approximation, despite the very different physics incorporated into the two approximations. The collective displacement described by the effective medium approximation is found to become the dominant contributor to the compliance of the network at high concentrations, but not by much: The tube diameters predicted by the two models remain comparable at values of $\rho L_p^2 \simeq 10^4$ typical of *F*-actin solutions, which are thus far the highest accessed in experiment. The elastic network approximation attempts to integrate these two approaches, by allowing both for continuum elastic deformations of the network and for motion of the test chain relative to that of the surrounding network, and so should provide a more realistic description of confinement than ei-

ther of the two simpler models.

Predictions of the elastic network approximation for the tube radius in tightly entangled *F*-actin solutions are in quantitative agreement (i.e., within a few tens of percent) with values of R_e in *F*-actin solutions obtained by fluoresence microscopy.

The theory of confinement presented here, when combined with the tube model of rheology presented previously, also predicts absolute magnitudes for the plateau moduli G in tightly entangled solutions. The comparison of predictions for G to rheological measurements on *F*-actin solutions is complicated by the fact that different experimental groups have not yet obtained quantitatively consistent results for the plateau modulus. The predictions of the elastic network modulus for the plateau modulus are found to be in good agreement with values measured by Hinner *et al.*, over about one decade in actin concentration, but are roughly a factor of 5 below those reported by the collaboration of Pollard and Xu and co-workers. A more quantitative test of the accuracy (or inaccuracy) of predictions for the plateau modulus will thus have to await resolution of the remaining experimental discrepancies in measurements using *F*-actin solutions, or the investigation of other model systems of tightly entangled chains.

ACKNOWLEDGMENTS

Helpful correspondence or conversations with Bernhard Hinner, Eric Sackmann, Josef Käs, Jay Tang, and Tony Maggs are gratefully acknowledged. I am particularly grateful to Josef Käs for providing and allowing me to reproduce the fluoresence microscopy data shown in Fig. 6, and to Bernhard Hinner and Eric Sackmann for the rheological data shown in Figs. 7 and 8. This work has been supported by National Science Foundation Grant No. DMR-9973976.

APPENDIX A: STATISTICAL MECHANICS OF A CONFINED POLYMER

This Appendix provides formal definitions for several single-chain thermodynamic potentials that may be used to characterize the topologically constrained equilibrium state of a single confined polymer.

Consider a network of $N+1$ chains that includes a test chain with contour $\mathbf{r}(s)$ and N medium chains with contours $\{\tilde{\mathbf{r}}_1(\tilde{s}), \ldots, \tilde{\mathbf{r}}_N(\tilde{s})\}$, in which the test chain is subjected to a transverse external force $\mathbf{f}(s)$. The canonical partition function for the entire topologically constrained network is given by a path integral

$$Z[\mathbf{f}] \equiv \int_{\text{accessible}} D[\mathbf{r}, \tilde{\mathbf{r}}_1, \ldots, \tilde{\mathbf{r}}_N] e^{-\{U_{bend}+U_{ext}\}/T}, \quad \text{(A1)}$$

in which $\int D[\mathbf{r}, \tilde{\mathbf{r}}_1, \ldots, \tilde{\mathbf{r}}_N]$ denotes a path integral over conformations of all $N+1$ chains, and in which the subscript ''accessible'' indicates that the path integral should be taken over only the subspace of topologically accessible microstates of the network. The bending energy U_{bend} is the sum of the single-chain bending energies of all $N+1$ chains, while the external potential U_{ext}, defined in Eq. (3), is a functional of the test chain contour alone.

By differentiating $\ln Z[\mathbf{f}]$ with respect to Fourier amplitudes $\mathbf{f}(q)$ of the external force, and then averaging over network topologies, it is straightforward to show that

$$\frac{\delta \overline{\ln Z[\mathbf{f}]}}{\delta f_\alpha(-q)} = \overline{\langle h_\alpha(q) \rangle}, \quad \text{(A2)}$$

$$\left. \frac{\delta^2 \overline{\ln Z[\mathbf{f}]}}{\delta f_\alpha(q) \delta f_\beta(-q)} \right|_{\mathbf{f}=\mathbf{0}} = \left. \frac{\delta \overline{\langle h_\alpha(q) \rangle}}{\delta f_\beta(q)} \right|_{\mathbf{f}=\mathbf{0}} = \overline{\langle h_\alpha(q) h_\beta(-q) \rangle_0}, \quad \text{(A3)}$$

where α and β are 2D Cartesian indices. By combining Eq. (A3) with Eq. (5) for $\overline{\langle h_\alpha(q) h_\beta(-q) \rangle_0}$, it may then be shown that

$$\left. \frac{\delta f_\alpha(q)}{\delta \overline{\langle h_\beta(q) \rangle}} \right|_{\overline{\langle \mathbf{h} \rangle}=\mathbf{0}} = [TL_p q^4 + \gamma(q)] \delta_{\alpha\beta}, \quad \text{(A4)}$$

where the left hand side is evaluated in the unperturbed equilibrium state, where $\mathbf{f}(s) = \overline{\langle \mathbf{h}(s) \rangle} = 0$.

The potential of mean force $A_{conf}[\mathbf{r}]$ is defined by a path integal

$$e^{-\beta A_{conf}[\mathbf{r}]} \equiv \int_{\text{accessible}} D[\tilde{\mathbf{r}}_1, \ldots, \tilde{\mathbf{r}}_N] e^{-\beta \Sigma_{i=1}^N U_{bend}[\tilde{\mathbf{r}}_i]} \quad \text{(A5)}$$

over topologically accessible conformations of the N medium chains, in which the test chain is constrained to a specified contour $\mathbf{r}(s)$, and in which the energy in the exponential is the total bending energy of the N medium chains alone. The only role of the test chain in this definition is thus to present an immoveable, uncrossable linelike obstacle to the other chains. The potential $A_{conf}[\mathbf{r}]$ depends upon the conformation of the test chain because changes in $\mathbf{r}(s)$ cause changes in the limits of integration (though not the integrand) in Eq. (A5). The probability $P[\mathbf{r}]$ that a fluctuating test chain will adopt a specified contour $\mathbf{r}(s)$ is given by the Boltzmann weight

$$P[\mathbf{r}] = Z^{-1} e^{-\{U_{bend}[\mathbf{r}] + A_{conf}[\mathbf{r}] + U_{ext}[\mathbf{r}]\}/T}, \quad \text{(A6)}$$

where $U_{bend}[\mathbf{r}]$ is the bending energy of the test chain alone.

In thermal equilibrium, the external force $\mathbf{f}$ exerted on a fluctuating test chain must, on average, be balanced by a combination of bending forces arising from the bending energy of the test chain and forces arising from collisions with neighboring chains. We may thus decompose $\mathbf{f}$ as a sum

$$\mathbf{f}(q) = \overline{\langle \mathbf{f}_{bend}(q) \rangle} + \overline{\langle \mathbf{f}_{conf}(q) \rangle}, \quad \text{(A7)}$$

where

$$\overline{\langle \mathbf{f}_{bend}(q) \rangle} \equiv \overline{\left\langle \frac{\delta U_{bend}[\mathbf{h}]}{\delta \mathbf{h}(-q)} \right\rangle}, \quad \text{(A8)}$$

$$\overline{\langle \mathbf{f}_{conf}(q)\rangle} \equiv \overline{\left\langle \frac{\delta A_{conf}[\mathbf{h}]}{\delta \mathbf{h}(-q)} \right\rangle}, \tag{A9}$$

are the average bending and confinement/collision forces exerted by the test chain. In the limit of weakly curved chains that is of interest here, we may approximate

$$\overline{\langle \mathbf{f}_{bend}(q)\rangle} \simeq TL_p q^4 \overline{\langle \mathbf{h}(q)\rangle}. \tag{A10}$$

Combining Eq. (A10) with Eq. (A4) immediately yields Eq. (14) for $\gamma(q)$ as a functional derivative $\gamma(q) = \delta f_{conf,\alpha}(q)/\delta\overline{\langle h_\alpha(q)\rangle}$.

The effective potential $\Gamma[\overline{\langle \mathbf{h}(s)\rangle}]$ is defined by the Legendre transform

$$\Gamma[\overline{\langle \mathbf{h}\rangle}] \equiv -T\,\overline{\ln(Z)} + \int ds \overline{\langle \mathbf{h}(s)\rangle} \cdot \mathbf{f}(s) \tag{A11}$$

of the topology-averaged free energy, and is a natural functional of the average displacement $\overline{\langle \mathbf{h}(s)\rangle}$. It may be shown by standard manipulations that

$$f_\alpha(q) = \frac{\delta\Gamma}{\delta\overline{\langle h_\alpha(-q)\rangle}}, \tag{A12}$$

where f is the total force on the chain. To separate the effect of interactions between chains from the effect of the intramolecular bending energy, it is convenient to decompose Γ as a sum $\Gamma = \Gamma_{bend} + \Gamma_{conf}$, in which Γ_{bend} is required to satisfy

$$\overline{\langle f_{bend,\alpha}(q)\rangle} \equiv \frac{\delta\Gamma_{bend}}{\delta\overline{\langle h_\alpha(-q)\rangle}}, \tag{A13}$$

and in which Γ_{conf} is required to satisfy the corresponding relation given in Eq. (15).

APPENDIX B: BCA EFFECTIVE POTENTIAL FOR A SEMIFLEXIBLE TEST CHAIN

Here, I present a binary collision approximation calculation of an effective potential for a semiflexible test chain. The calculation is similar to the one given in Sec. IV for a rigid test rod, except that here the test and medium chains are treated on a more equal footing, by allowing both chains to undergo transverse fluctuations around a preferred tube contour, as shown in Fig. 9. Consider interaction of a semiflexible test chain and medium chain with contours $\mathbf{r}(s)$ and $\tilde{\mathbf{r}}(\tilde{s})$, respectively, and define preferred tube contours $\langle \mathbf{r}(s)\rangle_t$ and $\langle \tilde{\mathbf{r}}(\tilde{s})\rangle_t$ for both chains; these are their average contours in the transparent state of the specified medium chain. In the absence of any external force on the test chain, the unperturbed preferred tube contours may be approximated near their point of closest approach by straight lines

$$\langle \mathbf{r}(s)\rangle_{t,0} = s\mathbf{u}, \tag{B1}$$

$$\langle \tilde{\mathbf{r}}(\tilde{s})\rangle_{t,0} = s_0\mathbf{u} + c_0\tilde{\mathbf{e}}_1 + \tilde{s}\,\tilde{\mathbf{u}}, \tag{B2}$$

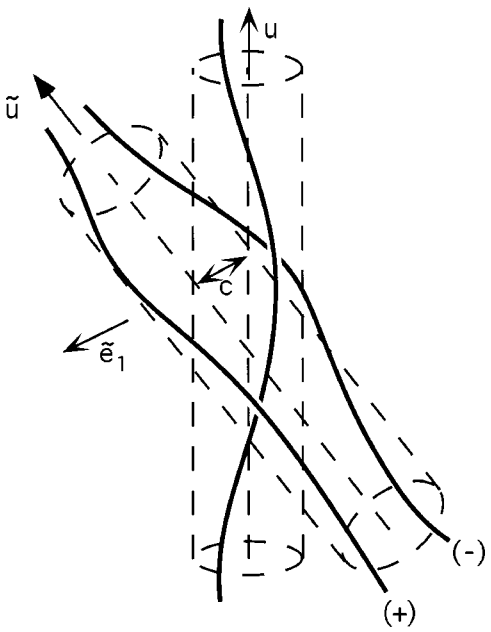

FIG. 9. Geometry for binary interaction of a fluctuating wormlike test chain with a preferred tube contour unit tangent **u** (vertical) near the point of closest approach to a preferred tube contour with unit tangent $\tilde{\mathbf{u}}$ of a nearby medium chain. The minimum distance between the preferred tube contours is $c = c_0 - \langle h_1\rangle$, where $\langle h_1\rangle = 0$ in the absence of an external force on the test chain.

where **u** and $\tilde{\mathbf{u}}$ are unit tangent vectors constructed parallel to these unperturbed tube contours at their point of closest approach, $\tilde{\mathbf{e}}_1$ is a unit vector perpendicular to **u** and $\tilde{\mathbf{u}}$, c_0 is the separation of the two tube contours at the point of closest approach, and $s_0\mathbf{u}$ is the position of the test chain contour at this point. Transverse displacements of the chain contours from these unperturbed tube contours are described by the fields

$$\mathbf{h}(s) \equiv \mathbf{r}(s) - \langle \mathbf{r}(s)\rangle_{t,0}, \tag{B3}$$

$$\tilde{\mathbf{h}}(\tilde{s}) \equiv \tilde{\mathbf{r}}(\tilde{s}) - \langle \tilde{\mathbf{r}}(\tilde{s})\rangle_{t,0}, \tag{B4}$$

which may be decomposed into Cartesian components

$$\mathbf{h}(s) = h_1(s)\tilde{\mathbf{e}}_1 + h_2\mathbf{e}_2, \tag{B5}$$

$$\tilde{\mathbf{h}}(\tilde{s}) = \tilde{h}_1(\tilde{s})\tilde{\mathbf{e}}_1 + \tilde{h}_2(\tilde{s})\tilde{\mathbf{e}}_2, \tag{B6}$$

where $\tilde{\mathbf{e}}_2$ is a unit vector that is perpendicular to both $\tilde{\mathbf{e}}_1$ and $\tilde{\mathbf{u}}$, and $\mathbf{e}_2$ is a unit vector perpendicular to $\tilde{\mathbf{e}}_1$ and **u**.

Consider a situation in which a spatially uniform force density **f** is applied to the test chain, so as to produce a uniform average displacement $\overline{\langle \mathbf{h}\rangle}_t$ in the tube (i.e., average) contour of the test chain. In the BCA, we asume that the application of this force causes no change in the preferred tube contour of the medium chain. When attempting to calculate the average displacement of the test chain, we must keep in mind that the average displacement of a semiflexible test chain at its point of closest approach to the tube contour

of a specified medium chain will generally be different from the average displacement $\overline{\langle \mathbf{h} \rangle}$ at a randomly chosen point along the test chain: The point of closest approach obviously has a special statistical status in the physical state of interest, since it is known that transverse fluctuations of the test chain are directly constrained at this point by the presence of the medium chain. I assume in what follows that the point of closest approach loses this special status in the transparent state, in which the test and medium chain can pass through each other, and thus approximate the average displacement of the preferred tube contour of the test chain at this point by the average displacement $\langle \mathbf{h} \rangle$ of the test chain at a randomly chosen point along its length, which may be taken to be far from the point of closest approach. The minimum separation of the two preferred tube contours (i.e., the thermal average contours in the transparent state) in the presence of an external force is then given, by analogy to Eq. (27), by $c = c_0 - \overline{\langle h_1 \rangle}$.

It is assumed that fluctuations of $\mathbf{h}$ and $\tilde{\mathbf{h}}$ at the point of closest approach are statistically independent in the transparent state, and that the probability distributions in this state may be approximated by Gaussians,

$$P(h_i) = \frac{1}{\sqrt{2\pi} R_e} e^{-(h_i - \overline{\langle h_i \rangle})^2 / 2R_e^2}, \tag{B7}$$

$$P(\tilde{h}_i) = \frac{1}{\sqrt{2\pi} R_e} e^{-\tilde{h}_i^2 / 2R_e^2} \tag{B8}$$

for Cartesian indices $i = 1$ or 2. The probability that the test chain and medium chain will be trapped in the + topological state, in which $\tilde{h}_1 > -c_0 + h_1$ at the point of closest approach, is equal to the probability of finding $\tilde{h}_1 > -c_0 + h_1$ in the transparent state when $\mathbf{f} = 0$, which is given by the double integral

$$p_+(c_0) = \int_{-\infty}^{\infty} dh_1 P(h_1) \int_{-c_0 + h_1}^{\infty} d\tilde{h}_1 P(\tilde{h}_1). \tag{B9}$$

The probabilities $p_+(c_0)$ and $p_-(c_0)$ of the + and − topological states may be expressed as

$$p_\pm(c_0) = \chi\left(\pm \frac{c_0}{R_e} \right), \tag{B10}$$

where

$$\chi(x) \equiv \int_{-\infty}^{\infty} \frac{dy}{\sqrt{2\pi}} e^{-y^2/2} \int_{-x+y}^{\infty} \frac{dz}{\sqrt{2\pi}} e^{-z^2/2}. \tag{B11}$$

Note that

$$\chi(x) = \Phi(x/\sqrt{2}), \tag{B12}$$

where $\Phi(x)$ is the normal distribution function defined in Eq. (32), as may be confirmed by differentiating $\chi(x)$ and carrying out the resulting Gaussian integral for $d\chi(x)/dx$ to show that $d\chi(x)/dx = d\Phi(x/\sqrt{2})/dx$.

In the physical situation of interest, where the test and medium chains are uncrossable, the probability distribution for values of h_1 at the point of closest approach between the tube contours of the test and medium chains, for a chain trapped in either the + or − topological state, is given by the Boltzmann weight

$$P_\pm(h_1) = \frac{\exp\{-(1/2R_e^2)(h_1 - \overline{\langle h_1 \rangle})^2 - \beta a_\pm(c_0 - h_1)\}}{\sqrt{2\pi R_e^2} \chi(c/R_e)}, \tag{B13}$$

where $a_\pm(c) = -T \ln \Phi(\pm c/R_e)$ is the binary interaction free energy given in Eq. (33), and where the normalization factor is chosen so as to guarantee that $\int P_\pm(h_1) = 1$. The average force exerted upon the medium chain, for a known topological state, averaged over fluctuations of both the medium and the test chains, is given by the integral

$$\langle f_\pm \rangle = \int dh_1 P_\pm(h_1) \left. \frac{\partial a_\pm}{\partial h_1} \right|_{c_0}. \tag{B14}$$

Using Eq. (B13) for $P_\pm$, it is straightforward to show that the rhs of Eq. (B14) may be expressed as a derivative,

$$\langle f_\pm \rangle = -T \frac{\partial}{\partial \overline{\langle h_1 \rangle}} \ln \chi(\pm c/R_e). \tag{B15}$$

The quantity $-T \ln \chi(\pm c/R_e)$ may thus be interpreted as a binary interaction contribution to the effective potential Γ_{conf} experienced by a semiflexible chain, in close analogy to the way that $a_\pm = -T \ln \Phi(\pm c/R_e)$ appears in Sec. IV as a contribution to the potential of mean force of a rigid test rod.

The rest of the calculation of the effective potential for a semiflexible test chain proceeds by close analogy to the corresponding calculation for a rigid test chain, and so is only outlined here. The average force $\overline{\langle \mathbf{f} \rangle}$ exerted by the test chain upon the medium chains may be expressed as the derivative $\overline{\langle \mathbf{f} \rangle} = (1/L) \partial \Gamma_{conf} / \partial \overline{\langle \mathbf{h} \rangle}$ of an effective potential Γ_{conf} that may be expressed in the BCA as an average of the binary interaction effective potential $-kT \ln \chi(\pm c/R_e)$ over all possible positions and orientations for the tube contours of nearby medium chains, and over both possible topological states for test and medium chains with known tube contours. Evaulating this average yields an expression for Γ_{conf} that is identical to that given in Eq. (41), except for the replacement of the function Φ by χ throughout the expression. Use of Eq. (B12) for $\chi(x)$ thus immediately yields Eq. (43) for Γ_{conf}.

APPENDIX C: FORCE DISTRIBUTION

Here, we consider a situation in which the test chain is subjected to a force $\mathbf{f}(s)$, and transmits an average force $\mathbf{f}_{conf}(s)$ to a relatively small set of primary medium chains. We attempt to describe the ensemble average $\mathbf{F}(\mathbf{r})$ for the force associated with collisions between these primary medium chains and the secondary medium chains that confine them. In doing so, we associate these secondary collision forces, as in the BCA, with the forces arising from a self-consistently determined confinement potential imposed on

each of the primary medium chains.

First consider the one-dimensional redistribution of forces along the length of a primary medium chain that is subjected to a force $\tilde{\mathbf{f}}(\tilde{s})$ arising from collisions with the test chain, where $\tilde{\mathbf{f}}(\tilde{s})$ lies in the plane perpendicular to the tube contour of the medium chain, and where $\tilde{s}$ is a contour distance along the medium chain. In practice, this force will be localized within a region of size R_e around the point of closest approach of the tube contours of the test chain and the medium chain of interest. The resulting average transverse displacement of the medium chain is given, in 1D Fourier space, by

$$\tilde{\mathbf{h}}(q)=\frac{1}{TL_pq^4+\gamma(q)}\tilde{\mathbf{f}}(q). \tag{C1}$$

The corresponding average force $\tilde{\mathbf{f}}_{conf}(q)=\gamma(q)\tilde{\mathbf{h}}(q)$ exerted on the confinement potential is given by

$$\tilde{\mathbf{f}}_{conf}(q)=\frac{\gamma(q)}{TL_pq^4+\gamma(q)}\tilde{\mathbf{f}}(q). \tag{C2}$$

By inverse Fourier transforming the above, we see that a localized force $\tilde{\mathbf{f}}$ exerted on a primary medium chain at point $\tilde{s}=0$ results, in this harmonic model, in a distributed force on the tube of the form $\tilde{\mathbf{f}}_{conf}(\tilde{s})=\tilde{\chi}(\tilde{s})\tilde{\mathbf{f}}$, where

$$\tilde{\chi}(\tilde{s})\equiv\int\frac{dq}{2\pi}\frac{\gamma(q)}{TL_pq^4+\gamma(q)}e^{-iq\tilde{s}} \tag{C3}$$

is a one-dimensional distribution function with a range of order L_e.

Now consider the 3D distribution of forces produced by the interaction of a test chain with nearby medium chains. Let $\mathbf{f}(\tilde{\mathbf{u}},s)$ be the average force exerted at point s along the test chain upon primary medium chains with orientation $\tilde{\mathbf{u}}$, so that $\mathbf{f}_{conf}=\int d\tilde{\mathbf{u}}\mathbf{f}(\tilde{\mathbf{u}},s)$. The corresponding spatial distribution $\mathbf{F}(\mathbf{r})$ of forces exerted by the primary chains upon their confinement potentials is given by

$$\mathbf{F}(\mathbf{r})=\int ds\int d\tilde{s}\int d\tilde{\mathbf{u}}\,\delta(\tilde{\mathbf{u}}\tilde{s}+s\mathbf{u}-\mathbf{r})\tilde{\chi}(\tilde{s})\mathbf{f}(\tilde{\mathbf{u}},s), \tag{C4}$$

where $\tilde{s}$ is a distance measured along the medium chain from the point of collision with the test chain. Fourier transforming the above gives

$$\mathbf{F}(\mathbf{k})=\int d\tilde{\mathbf{u}}\frac{\gamma(q)}{TL_pq^4+\gamma(q)}\mathbf{f}(\tilde{\mathbf{u}},q), \tag{C5}$$

where $q\equiv\mathbf{k}\cdot\tilde{\mathbf{u}}$, and where $\mathbf{f}(\tilde{\mathbf{u}},q)$ and $\tilde{\chi}(q)$ are the 1D Fourier transforms of $\mathbf{f}(\tilde{\mathbf{u}},s)$ and $\tilde{\chi}(\tilde{s})$, respectively.

Two further approximations are now introduced purely for reasons of mathematical simplicity.

(i) The force $\mathbf{f}(\mathbf{u},s)$ is approximated by a function

$$\mathbf{f}(\tilde{\mathbf{u}},s)=\mathbf{f}_{conf}(s)/(2\pi) \tag{C6}$$

that is independent of $\tilde{\mathbf{u}}$, thus assuming that the force exerted by the test chain on its surroundings is distributed randomly to medium chains with all orientations. By this ''preaveraging'' of $\mathbf{f}(\tilde{\mathbf{u}},s)$ with respect to $\mathbf{u}$, we obtain a force of the form given in Eq. (55) with a transformed 3D distribution function

$$\chi(\mathbf{k})=\int\frac{d\tilde{\mathbf{u}}}{2\pi}\frac{\gamma(q)}{TL_pq^4+\gamma(q)}, \tag{C7}$$

where $q\equiv\mathbf{k}\cdot\tilde{\mathbf{u}}$.

(ii) The function $\gamma(q)$ is approximated for this purpose by a q-independent constant $\gamma(q)=TL_pq_e^4$, with a value $q_e=2^{3/2}/L_e$ chosen so as to return the correct value for L_e when this approximation for $\gamma(q)$ is used in Eq. (10).

Equation (56) for $\chi(\mathbf{k})$ is obtained by using this last approximation for $\gamma(q)$ in Eq. (C7).

[1] T. Odijk, Macromolecules **16**, 1340 (1983).
[2] M. Doi, J. Polym. Sci., Polym. Symp. **73**, 93 (1985).
[3] A. N. Semenov, J. Chem. Soc., Faraday Trans. 2 **86**, 317 (1986).
[4] R. Granek, J. Phys. II **7**, 1761 (1997).
[5] F. C. MacKintosh, P. A. Janmey, and J. Käs, Phys. Rev. Lett. **75**, 4425 (1995).
[6] H. Isambert and A. C. Maggs, Macromolecules **29**, 1036 (1996).
[7] A. C. Maggs, Phys. Rev. E **55**, 7396 (1997).
[8] A. C. Maggs, Phys. Rev. E **57**, 2091 (1998).
[9] F. Gittes and F. C. MacKintosh, Phys. Rev. E **58**, 1241 (1998).
[10] D. C. Morse, Phys. Rev. E **58**, 1237 (1998).
[11] D. C. Morse, Macromolecules **31**, 7030 (1998).
[12] D. C. Morse, Macromolecules **31**, 7044 (1998).
[13] D. C. Morse, Macromolecules **32**, 5934 (1998).
[14] D. C. Morse (unpublished).
[15] M. Doi and S. F. Edwards, *The Theory of Polymer Dynamics* (Oxford University Press, London, 1986).
[16] P. G. de Gennes, Macromolecules **9**, 587 (1976).
[17] M. Adam and M. Delsanti, J. Phys. (France) **44**, 1185 (1983); Macromolecules **28**, 927 (1995).
[18] M. Adam and M. Delsanti, J. Phys. (France) **45**, 1513 (1984); Macromolecules **18**, 1760 (1985).
[19] R. Colby and M. Rubinstein, Macromolecules **23**, 2753 (1990); R. Colby, M. Rubinstein, and J.-L. Viovy, *ibid.* **25**, 996 (1992); R. Colby, M. Rubinstein, and M. Daoud, J. Phys. II **4**, 1299 (1994).
[20] L. J. Fetters, D. J. Lohse, D. Richter, T. A. Witten, and A. Zirkel, Macromolecules **17**, 4640 (1994).

[21] J. Käs, H. Strey, and E. Sackmann, Nature (London) **368**, 226 (1994).
[22] J. Käs, H. Strey, J. X. Tang, D. Finger, R. Ezzell, E. Sackmann, and P. Janmey, Biophys. J. **70**, 609 (1996).
[23] F. Gittes, B. Mickey, J. Nettleton, and J. Howard, J. Cell Biol. **120**, 923 (1993).
[24] A. Ott, M. Magnasco, A. Simon, and A. Libchaber, Phys. Rev. E **48**, 1642 (1993).
[25] H. Isambert, P. Venier, A. C. Maggs, A. Fattoum, R. Kassab, D. Pantaloni, and M.-F. Carlier, J. Biol. Chem. **270**, 11 437 (1995).
[26] P. A. Janmey, S. Hvidt, J. Käs, D. Lerche, A. C. Maggs, E. Sackmann, M. Schliwa, and T. P. Stossel, J. Biol. Chem. **269**, 32 503 (1994).
[27] D. H. Wachsstock, W. H. Schwarz, and T. D. Pollard, Biophys. J. **65**, 205 (1993); **66**, 801 (1994).
[28] J. Xu, A. Palmer, and D. Wirtz, Macromolecules **31**, 6486 (1998).
[29] J. Xu, W. H. Schwarz, J. Käs, T. P. Stossel, P. A. Janmey, and T. D. Pollard, Biophys. J. **74**, 2731 (1998).
[30] R. Ruddies, W. H. Goldman, G. Isenberg, and E. Sackmann, Eur. Biophys. J. **22**, 309 (1993).
[31] B. Hinner, M. Tempel, E. Sackmann, K. Kroy, and E. Frey, Phys. Rev. Lett. **81**, 2614 (1998).
[32] J. X. Tang, P. A. Janmey, T. P. Stossel, and T. Ito, Biophys. J. **76**, 2208 (1999).
[33] S. F. Edwards and K. E. Evans, Trans. Faraday Soc. **78**, 113 (1982).
[34] Z. Bu, P. S. Russo, D. L. Tipton, and I. Negulescu, Macromolecules **27**, 6871 (1994).
[35] B. Hinner (private communication).